

Deflection angle with electromagnetic interaction and Gravitational-electromagnetic dual lensing

Xiaoge Xu,¹ Tingyuan Jiang,¹ and Junji Jia^{2,*}

¹*School of Physics and Technology, Wuhan University, Wuhan, 430072, China*

²*Center for Astrophysics & MOE Key Laboratory of Artificial Micro- and Nano-structures, School of Physics and Technology, Wuhan University, Wuhan, 430072, China*

(Dated: July 12, 2022)

The trajectory deflection and gravitational-electromagnetic dual lensing (GEL) of charged signal in general charged static and spherically symmetric spacetimes are considered in this work. We showed that the perturbative approach previously developed for neutral particles can be extended to the electromagnetic interaction case. The deflection angle still takes a (quasi-)series form and the finite distance effect of both the source and observer can be taken into account. Comparing to pure gravitational case, the apparent angles of the images in the GEL, their magnifications and time delay all receive the electromagnetic corrections starting from the first non-trivial order. The sign and relative size of the leading corrections are determined by $\sim \frac{Q}{M} \frac{q}{E}$ where M , Q , q , E are the spacetime mass and charge, and signal particle charge and energy respectively. It is found that for $qQ > 0$ (or < 0), the electromagnetic interaction will decrease (or increase) the deflection angle, and in GEL the impact parameters, apparent angles, magnifications and total travel time for each image. The time delay is increased for small β and $qQ > 0$, and otherwise always increased regardless the sign of qQ . The results are then applied to the deflection and GEL of charged protons in cosmic rays in Reissner-Nordstrom, charged dilaton and charged Horndeski spacetimes.

Keywords: Deflection angle, Gravitational lensing, charged particle, timelike particles

I. INTRODUCTION

Deflection of light in gravitational field was one of the most important supporting evidence in the development of General Relativity [1]. It is the foundation of gravitational lensing (GL), which itself has also become a very powerful tool in astrophysics and cosmology. GL can be used to investigate properties of the supernova [2], coevolution of galaxies and supermassive black holes (SMBHs) [3], mass distributions of galaxy clusters [4] and the Universe [5], cosmological parameters [6, 7] and dark matter and energy [8, 9].

Besides the usual light rays, other types of signals such as neutrinos, gravitational waves (GW) and cosmic rays (CR) can also travel across large scale distance and become messengers of their sources, carry information about themselves and the spacetime they passed. With the discovery of SN 1987A neutrinos [10, 11] and the recent neutrinos from blazar TXS 0506+056 [12, 13], the more recent GWs [14–17] and multimessenger event [18], neutrinos and GWs are now recognized as important tools in astrophysical observations. On the other hand, the CRs have an even longer observational history [19] and it has become more clear in recent years that CRs with ultra-high energies (UHE) are composed of charged massive particles of proton and heavier nucleus [20].

Previously, trajectory deflection and GL of neutral massive signals, including neutrinos and GWs in some gravitational theories beyond GR, have been studied by many researchers. The dependence of the deflection an-

gle and GL observables on the general metric functions and signal properties have been studied in the weak field limit using both the perturbative method [21–29] and Gauss-Bonnet theorem method [30–37]. Recently, there is a resurgence of interest to study the deflection of charged massive particles (CMP) in charged spacetimes [32, 38, 39]. Although there might be intergalactic magnetic field that can cause chaotic motions of these signals, not all inter-galactic space carry (strong) magnetic field. Particularly, for CMP with UHE, deflection due to extragalactic magnetic field are expected to be small [20].

In this work we will study the deflection and the dual gravitational and electromagnetic lensing (GEL) of CMP in general charged static and spherical symmetric (SSS) spacetimes. We will investigate whether the perturbative method that was developed previously for neutral particles in general SSS or stationary axisymmetric spacetimes in the weak field limit [24–28] can be extended to the case with electromagnetic interaction. It turns out that the extension is possible with only a small modification of the derivation process (see Sec. II). Using this method we will compute the deflection angle of CMP in general charged SSS spacetime with finite distance effect of the source and detector and the electromagnetic interaction taken into account. The image apparent angles and time delay in the GEL, including the leading order contribution from the electromagnetic interaction, will also be given (Sec. III). We then apply the results to the Reissner-Nordstrom, Gibbons-Maeda-Garfinkle-Horowitz-Strominger (GMGHS) [40–42] and charged Horndeski [43] spacetimes to verify the validity of the result and show more clearly the effect of the electromagnetic interaction on various quantities (Sec. IV). We use the natural units $G = c = 1/(4\pi\epsilon_0) = 1$ in this

* Corresponding author: junjijia@whu.edu.cn

work.

II. THE PERTURBATIVE METHOD

We start from the SSS metric with line element

$$ds^2 = -A(r)dt^2 + B(r)dr^2 + C(r)(d\theta^2 + \sin^2\theta d\phi^2) \quad (1)$$

where (t, r, θ, ϕ) are the coordinates and $A(r)$, $B(r)$ and $C(r)$ are the metric functions. We assume that the spacetime only possess a known SSS electric field but no magnetic field. Therefore the field can be described by the four-potential $A_\mu(r)$ with $A_0 \neq 0$, $A_i = 0$ ($i = 1, 2, 3$).

The motion of charged particle with mass m and charge q under both gravity and electric interaction is described by the Lorentz equation [44]

$$\frac{d^2x^\rho}{d\tau^2} + \Gamma_{\mu\nu}^\rho \frac{dx^\mu}{d\tau} \frac{dx^\nu}{d\tau} = \frac{q}{m} F_\mu^\rho \frac{dx^\mu}{d\tau}, \quad (2)$$

where τ is the proper time or affine parameter of the particle, and $F_{\mu\nu} = \partial_\mu A_\nu - \partial_\nu A_\mu$ is the electromagnetic field strength. From this we can see that the motion of the particle no longer follows a geodesic in the background spacetime.

Previously, for neutral particles, we have computed the deflection angle using a perturbative method developed in Ref. [24, 26]. It turns out this method can be extended to the current case of charged particles under dual influence of gravity and electric interactions, with a small modification at essentially only one place in the equations. Here we will briefly recap the perturbative method and point out this modification, and show that this method is applicable to all SSS spacetime with arbitrary electric potential $A_0(r)$.

First of all, the time, angular and radial components of the Eqs. (2), after first integrals, become

$$\dot{t} = \frac{E + qA_0}{mA}, \quad (3)$$

$$\dot{\phi} = \frac{L}{mC}, \quad (4)$$

$$\dot{r}^2 = \frac{[(E + qA_0)^2 - m^2A]C - L^2A}{m^2ABC}, \quad (5)$$

where without losing any generality we have set the trajectory to be in the equator plane, i.e., $\theta = \pi/2$. Here the L and E are constants of first integrals allowed by the SSS symmetry and can be interpreted as the angular momentum and energy of the particle in an asymptotically flat spacetime. L can be related to the trajectory's minimal radius r_0 using Eq. (5), i.e. $\dot{r}|_{r=r_0} = 0$, to find

$$L = \sqrt{[(E + qA_0)^2 - m^2A(r_0)]C(r_0)/A(r_0)}. \quad (6)$$

Comparing to the case without the electric interaction [24], the effect of the charge manifests in Eqs. (3)-(6) through the term involving qA_0 . In asymptotically flat

spacetimes (on which this work concentrates), L and E can also be related to the signal's impact parameter b and the asymptotic velocity v by

$$L = |\mathbf{r} \times \mathbf{p}| = \frac{mv}{\sqrt{1-v^2}}b, \quad E = \frac{m}{\sqrt{1-v^2}}. \quad (7)$$

From Eqs. (3) to (5), the change of the angular coordinates $\Delta\phi$ from a source located at (r_s, ϕ_s) to the detector located at (r_d, ϕ_d) (see Fig. 1) becomes

$$\Delta\phi = \left[\int_{r_0}^{r_s} + \int_{r_0}^{r_d} \right] \sqrt{\frac{B}{C}} \frac{L}{\sqrt{[(E + qA_0)^2/A - m^2]C - L^2}} dr, \quad (8)$$

while the total flight time Δt becomes

$$\Delta t = \left[\int_{r_0}^{r_s} + \int_{r_0}^{r_d} \right] \frac{\sqrt{BC}}{A} \frac{E + qA_0}{\sqrt{[(E + qA_0)^2/A - m^2]C - L^2}} dr. \quad (9)$$

The integrals (8) and (9) usually can not be explicitly carried out for general SSS metric and therefore require an perturbative technique to find their approximations.

To precede, one can replace the L , E and r_0 in Eqs. (8) and (9) by b and v . Solving b from Eq. (7) and using Eq. (6), we have

$$\frac{1}{b} = \frac{\sqrt{E^2 - m^2}}{\sqrt{(E + qA_0(r_0))^2 - m^2A(r_0)}} \sqrt{\frac{A(r_0)}{C(r_0)}} \quad (10)$$

$$\equiv p \left(\frac{1}{r_0} \right). \quad (11)$$

Here we have defined the right hand side of Eq. (10) as a function p of $1/r_0$. For later usage, we will denote the inverse function of $p(x)$ as $w(x)$. We emphasize that once the metric functions and four-potential are known, the functions $p(x)$ will be explicitly known too. Although obtaining the analytical form of a function's inverse function, in this case $w(x)$, can sometimes be difficult, its series form can always be obtained using the Lagrange inversion theorem. And this series form of $w(x)$ is all we need for later perturbative computations.

One of the difficulties in the integration of Eq. (8) and (9) comes from the fact that the minimal radius r_0 , which is usually difficult to link to observables but often used as expansion parameter, appears in the lower limit. To solve this problem, in Ref. [24, 26], we have proposed the change of variables from r to u which are linked by $w(x)$ (but without particle charge there). In the current situation, it appears that a similar change of variables from r to u can still be used as long as we use the updated $p(x)$ and $w(x)$ given in Eq. (11), i.e.,

$$\frac{1}{r} = w \left(\frac{u}{b} \right) \text{ or equivalently } r = 1/w \left(\frac{u}{b} \right). \quad (12)$$

With this and also using Eqs. (6) and (11), the integral limits and various terms in the integrand of Eq. (8) and (9) can be transformed to (also see [26])

$$r_0 \rightarrow 1, \quad r_{s,d} \rightarrow b \cdot p \left(\frac{1}{r_{s,d}} \right), \quad (13a)$$

$$dr \rightarrow -\frac{1}{p'(w)w^2} \frac{1}{b} du, \quad (13b)$$

$$\sqrt{\frac{B}{C}} \rightarrow \sqrt{\frac{B(1/w)}{C(1/w)}}, \quad (13c)$$

$$\frac{L}{\sqrt{[(E + qA_0)^2/A - m^2]C - L^2}} \rightarrow \frac{u}{\sqrt{1 - u^2}}. \quad (13d)$$

Combining the right hand sides of Eq. (13), the $\Delta\phi$ becomes

$$\Delta\phi = \left[\int_{\sin\theta_s}^1 + \int_{\sin\theta_d}^1 \right] y\left(\frac{u}{b}\right) \frac{du}{\sqrt{1 - u^2}} \quad (14)$$

where we have collectively denoted part of the integrand as

$$y\left(\frac{u}{b}\right) = \sqrt{\frac{B(1/w)}{C(1/w)}} \frac{1}{p'(w)w^2} \frac{u}{b}, \quad \text{with } w = w\left(\frac{u}{b}\right) \quad (15)$$

Note in Eqs. (14)

$$\theta_s = \arcsin \left[b \cdot p\left(\frac{1}{r_s}\right) \right], \quad \theta_d = \arcsin \left[b \cdot p\left(\frac{1}{r_d}\right) \right] \quad (16)$$

are respectively the apparent angles of the signal at the source and detector [24]. Similar to $\Delta\phi$, the total travel time Δt in Eq. (9) becomes

$$\Delta t = \left[\int_{\sin\theta_s}^1 + \int_{\sin\theta_d}^1 \right] z\left(\frac{u}{b}\right) \frac{du}{u\sqrt{1 - u^2}} \quad (17)$$

where

$$z\left(\frac{u}{b}\right) = \frac{\sqrt{B(1/w)C(1/w)}}{A(1/w)} \frac{u}{b} \frac{1}{v} \frac{1}{p'(w)w^2} \frac{u}{b} \times \left[1 + \hat{q}A_0(1/w)\sqrt{1 - v^2} \right] \quad (18)$$

where $\hat{q} \equiv q/m$ is the charge-mass ratio of the signal particle.

Now we restrict ourselves to the weak field limit, in which the impact parameter is much larger than the characteristic mass of the spacetime. Therefore in this limit we can expand respectively the $y\left(\frac{u}{b}\right)$ factor in Eq. (14) and $z\left(\frac{u}{b}\right)$ factor in Eq. (17) into series of $\frac{u}{b}$

$$y\left(\frac{u}{b}\right) = \sum_{n=0} y_n \left(\frac{u}{b}\right)^n, \quad (19)$$

$$z\left(\frac{u}{b}\right) = \sum_{n=-1} z_n \left(\frac{u}{b}\right)^n, \quad (20)$$

where the two series start respectively from $n = 0$ and $n = -1$ because of the form of the metric functions and electric potential given in Eq. (21).

The important point is that these coefficients y_n in Eq. (23) and z_n in Eq. (24) can always be expressed in terms of the coefficients of the asymptotic expansions of the

metric functions and the electric potential, which we will assume to be

$$A(r) = \sum_{n=0}^{\infty} \frac{a_n}{r^n}, \quad B(r) = \sum_{n=0}^{\infty} \frac{b_n}{r^n}, \quad C(r) = r^2 \sum_{n=0}^{\infty} \frac{c_n}{r^n}, \quad (21)$$

$$A_0(r) = \sum_{n=1}^{\infty} \frac{a_{0n}}{r^n}.$$

Without losing any generality, we can always choose $a_0 = b_0 = c_0 = 1$ and identify $a_1 = -2M$, $a_{01} = -Q$ where M and Q are respectively the ADM mass and total charge of the spacetimes. In principle, we can even set $C(r) = r^2$ exactly because the allowed change of the coordinates. However for the moment we will allow general c_n ($n \geq 1$) because some works presented their $C(r)$ in other forms. Using the expansions (21) in Eq. (11), we can obtain the series form of function $p(x)$ as

$$p(x) = x + \left(\frac{a_1}{2v^2} - \frac{c_1}{2} - \frac{a_{01}\hat{q}\sqrt{1 - v^2}}{v^2} \right) x^2 + \mathcal{O}(x)^3. \quad (22)$$

Inverting this series, we can obtain a series form of $w(x)$ and then substituting it together with Eq. (21) into Eqs. (15) and (18), we can further expand them according to Eqs. (23) and (24) and the first few coefficients are found to be

$$y_0 = 1 \quad (23a)$$

$$y_1 = -\frac{a_1}{2v^2} + \frac{b_1}{2} + \frac{a_{01}\hat{q}\sqrt{1 - v^2}}{v^2} \quad (23b)$$

$$y_2 = -\frac{1}{2v^2} [a_1(b_1 + c_1 - 2a_1) + 2a_2] - \frac{1}{8}(b_1 + c_1)^2 + \frac{1}{2}(b_2 + c_2) + [(b_1 + c_1 - 2a_1)a_{01} + 2a_{02}] \frac{\hat{q}\sqrt{1 - v^2}}{v^2} + \left(\frac{1}{v^2} - 1 \right) a_{01}^2 \hat{q}^2, \quad (23c)$$

and

$$z_{-1} = \frac{1}{v} \quad (24a)$$

$$z_0 = \frac{1}{v} \left(-a_1 + \frac{b_1}{2} + \frac{a_1}{2v^2} \right) + \left(1 - \frac{1}{v^2} \right) \frac{a_{01}\hat{q}\sqrt{1 - v^2}}{v} \quad (24b)$$

$$z_1 = \frac{1}{2v} [a_1(2a_1 - b_1 - c_1) - 2a_2 + b_2 + c_2] - \frac{1}{8v}(b_1 - c_1)^2 + [(b_1 + c_1 - 2a_1) + 2a_{02}] \frac{a_{01}\hat{q}\sqrt{1 - v^2}}{2v}. \quad (24c)$$

Higher order coefficients can also be easily obtained but they are only shown in Appendix B for their excessive length.

A few comments are in order here. Firstly, setting $q = 0$ in Eqs. (23) and (24), the y_n and z_n reduces to

the case of neutral particles (without electromagnetic interaction), which agrees with results in Ref. [24, 26]. Secondly, the electromagnetic interaction affects both $\Delta\phi$ and Δt from the first non-trivial orders ($n = 1$ and $n = 0$ respectively) through a_{01} , in contrast to the gravitational effect of spacetime charge which only appears from the second non-trivial order through a_2 or b_2 (see Eq. (48) for their values in the RN spacetime). Thirdly, we see that all terms involving the potential $A_0(r)$ or equivalently a_{0n} are multiplied by positive powers of q , and vice versa (also see Eq. (B1)). This implies that the electromagnetic interaction between the particle and central lens contributes to the deflection angle or flight time only through these terms. Furthermore, from Eqs. (23) and (24) one observes that quantitatively the electromagnetic interaction correction is proportional to $\sim \hat{q}\sqrt{1-v^2} = \frac{q}{m} \cdot \frac{m}{E} = q/E$, i.e, the inverse of the signals' *rigidity*. Although for relativistic particles its m/E is small and the charge of spacetime is also expected to be (much) smaller than its mass, the charge-mass ratio q/m , when converted to a dimensionless quantity, is actually very large, being 1.11×10^{18} for protons and 2.04×10^{21} for electrons. Therefore the electromagnetic correction terms are not necessarily small comparing to other terms in the coefficients. This is a reflection of the very fact that the electromagnetic interaction strength is much stronger than that of the gravitational interaction. Because of this possible largeness and the fact that we are carrying out a *perturbative* computation, the validity of the method developed in this work requires the condition that

$$\mathcal{O}\left(a_{01}\hat{q}\sqrt{1-v^2}\right) \approx \mathcal{O}\left(\frac{a_{01}q}{E}\right) < \mathcal{O}(b). \quad (25)$$

Finally, the $\Delta\phi$ of massless charged particles can be obtained by systematically replacing $\hat{q}\sqrt{1-v^2} \rightarrow q/E$ and then taking the $v \rightarrow 1$ limit in Eq. (19).

Substituting Eqs. (23) and (24) into Eq. (14) and (17), $\Delta\phi$ and Δt both become sums of a series of integrals of them form

$$I_n(\theta_i) = \int_{\sin\theta_i}^1 \frac{u^n}{\sqrt{1-u^2}} du \quad (26)$$

which can always be integrated into elementary functions and their explicit forms are given in Eq. (A2) in Appendix A. Consequently we found an effective way to approximate the initial $\Delta\phi$ and Δt

$$\Delta\phi = \sum_{i=s,d} \sum_{n=0}^{\infty} y_n \frac{I_n(\theta_i)}{b^n}, \quad (27)$$

$$\Delta t = \sum_{i=s,d} \sum_{n=-1}^{\infty} z_n \frac{I_{n-1}(\theta_i)}{b^n}. \quad (28)$$

For the change of the angular coordinate, to the first three orders, Eq. (27) is

$$\Delta\phi = \sum_{i=s,d} \left\{ \left(\frac{\pi}{2} - \theta_i \right) y_0 + c_i \frac{y_1}{b} + \frac{1}{4} (\pi + 2s_i c_i - 2\theta_i) \frac{y_2}{b^2} \right.$$

$$\left. + \mathcal{O}\left(\frac{M}{b}\right)^3 \right\}, \quad (29)$$

where y_n ($n = 0, 1, 2$) are given in Eq. (23) and $s_i = \sin\theta_i$ and $c_i = \cos\theta_i$ ($i = s, d$). It is seen that the leading trivial order result with $y_0 = 1$ is given by $\pi - \theta_s - \theta_d$, which corresponds to the straight trajectory result. For the first non-trivial order result, i.e. y_1/b , using Eq. (23b), it is seen that comparing to the neutral signal case, $\Delta\phi$ receives a correction from the electromagnetic interaction, which as pointed out previously is not necessarily small. The finite distance effect of the source and detector is manifest through terms involving θ_i ($i = s, d$) defined in Eq. (16). To see the finite distance effect more clearly, we can expand I_n in the small b/r_i limit. Using the first few of these expansions given in Eq. (A4), $\Delta\phi$ is further transformed to

$$\begin{aligned} \Delta\phi = \sum_{i=s,d} & \left\{ \frac{\pi}{2} y_0 + \frac{y_1}{b} + \frac{\pi}{4} \frac{y_2}{b^2} - \frac{b}{r_i} y_0 \right. \\ & \left. - \frac{b}{r_i^2} \left[\left(\frac{a_1}{2v^2} - \frac{c_1}{2} - \frac{a_{01}\hat{q}\sqrt{1-v^2}}{v^2} \right) y_0 + y_1 \right] \right. \\ & \left. + \mathcal{O}\left(\frac{M}{b}\right)^3 \right\}, \quad (30) \end{aligned}$$

The first three terms of this result is the infinite distance deflection angle with the electromagnetic interaction taken into account.

III. GEL AND TIME DELAY

Now with results (27) and (28), in principle we can simply obtain $\Delta\phi$ and Δt for any specific metric functions and four-potential. Before going to specific spacetimes however, in this section we will set up the GEL equations in general charged SSS spacetimes to solve the apparent angles of images and the time delay between them.

The setup of the GEL is illustrated in Fig. 1. Since our change of the angular coordinate (27) is applicable to source and detectors at finite distance, we can use it to establish an exact GEL equation linking the source angular position β_L and two impact parameter b_{\pm} from each side of the lens. With b_{\pm} solved from this equation, then using Eq. (16) we can find the corresponding apparent angles of the images, after which their magnifications and furthermore the time delays between the two signals can also be solved.

The exact GEL equation is nothing but the following relation, or equivalently the very definition of $\Delta\phi$

$$\Delta\phi(b_{\pm}) = \pi \pm \beta_L \quad (31)$$

where the $+$ and $-$ signs correspond to rays propagating counter-clockwisely and clockwisely respectively (see Fig. 1). Substituting $\Delta\phi$ in Eq. (30) truncated to the first

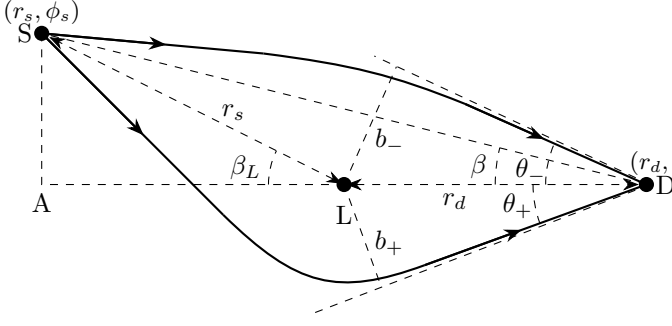


FIG. 1. The GEL setup. The source is located at angle β_L and β respectively with respect to the lens and detector against the lens-detector axis. The impact parameters and the corresponding apparent angles corresponding to counter-clockwise and clockwise trajectories are labeled as b_+ and θ_+ , and b_- and θ_- respectively.

non-trivial orders (i.e. $(M/b)^1$ and $(b/r_i)^1$) into the above equation, this equation becomes

$$\pi + \left(b_1 - \frac{a_1}{v^2} + \frac{2a_{01}\hat{q}\sqrt{1-v^2}}{v^2} \right) \frac{1}{b} - b \left(\frac{1}{r_s} + \frac{1}{r_d} \right) = \pi \pm \beta_L. \quad (32)$$

From this, one can solve the two impact parameters

$$b_{\pm} = \frac{\beta_L r_d r_s}{2(r_d + r_s)} \left[\sqrt{1 + \eta} \mp 1 \right] \quad (33)$$

where

$$\eta = \frac{8(r_d + r_s)}{\beta_L^2 r_d r_s} \left(-\frac{a_1}{2v^2} + \frac{b_1}{2} + \frac{a_{01}\hat{q}\sqrt{1-v^2}}{v^2} \right). \quad (34)$$

Comparing to the corresponding result of neutral particles (Eq. (30) of Ref. [25]), the electromagnetic interaction term $a_{01}\hat{q}$ now has a non-trivial contribution to b_{\pm} . Since $a_1 = -2M$ and $a_{01} = -Q$, we see from Eq. (34) that if $\text{sign}(qQ) = 1$ (or -1), i.e., the electromagnetic interaction between the particle and the lens is repulsive (or attractive), then η will be smaller (or larger) than the neutral particle case. Using Eq. (33), this implies that electric repulsion (or attraction) between the signal and lens charges will force the desired impact parameters from both sides to decrease (or increase).

For the apparent angles of the images, from Eq. (16) and using (22), to the second order of $1/r_d$, we have

$$\theta_{\pm} = b_{\pm} \left[\frac{1}{r_d} + \left(\frac{a_1}{2v^2} - \frac{c_1}{2} - \frac{a_{01}\hat{q}\sqrt{1-v^2}}{v^2} \right) \frac{1}{r_d^2} \right] \quad (35)$$

where b_{\pm} is given by Eq. (33). For $\beta_L = 0 = \beta$, the corresponding Einstein ring has an angular size

$$\theta_E = \sqrt{\frac{2r_s}{r_d(r_s + r_d)} \left(-\frac{a_1}{2v^2} + \frac{b_1}{2} + \frac{a_{01}\hat{q}\sqrt{1-v^2}}{v^2} \right)}. \quad (36)$$

Since the second order term of θ_{\pm} is much smaller than the leading $1/r_d$ order term, the apparent angles θ_{\pm} and the corresponding θ_E will both be affected by the electromagnetic interaction in the same manner as b_{\pm} was affected. That is, $\text{sign}(qQ) = 1$ (or -1) will lead to smaller (or larger) apparent angle of the images. The deviation of the trajectories of charges with different signs from that of neutral particles, and the change of the corresponding b_{\pm} , θ_{\pm} , are qualitatively represented in Fig. 2 by the dashed ($\text{sign}(qQ) = 1$) and dotted ($\text{sign}(qQ) = -1$) lines.

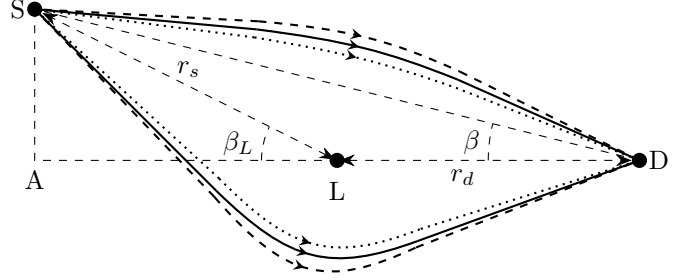


FIG. 2. The GEL setup for signal with $\text{sign}(qQ) = -1$ (dashed), neutral (solid) and $\text{sign}(qQ) = 1$ (dotted). The impact parameters, apparent angles of the images and Einstein radius will all be larger (or smaller) for signal with $\text{sign}(qQ) = -1$ (or 1) comparing to neutral particles.

To compute the magnification of the images, which is defined as

$$\mu_{\pm} = \left| \frac{\theta_{\pm}}{\beta} \frac{d\theta_{\pm}}{d\beta} \right|, \quad (37)$$

we should link the apparent angle θ_{\pm} with β (see Fig. 1). This can be realized by the geometrical relation in triangles $\triangle SAL$ and $\triangle SAD$

$$r_s \sin \beta_L = (r_d + r_s \cos \beta_L) \tan \beta. \quad (38)$$

Therefore after substituting Eq. (35) into Eq. (37) and using Eq. (38), the magnifications become

$$\mu_{\pm} = \left| \frac{\theta_{\pm}}{\beta} \frac{d\theta_{\pm}}{d\beta_L} \frac{d\beta_L}{d\beta} \right| = \frac{u_{\beta}^2 + 2}{2u_{\beta} \sqrt{u_{\beta}^2 + 4}} \mp \frac{1}{2} \quad (39)$$

where $u_{\beta} = \beta/\theta_E$. Formally this takes the same form as the magnification in simple Schwarzschild BH lensing case [45], but note the θ_E is now given by Eq. (36), containing electromagnetic interaction. Clearly, a larger θ_E (i.e. $\text{sign}(qQ) = -1$) causes a smaller u_{β} , which in turn causes the magnification of both images to become larger than the neutral signal case. Similarly, for charges with $\text{sign}(qQ) = 1$, both magnifications will be smaller than the neutral case.

With the two impact parameters b_{\pm} known in Eq. (33), using the travel time result (28) with the first three I_n ($n = -1, 0, 1$) given in Eq. (A4), one can subtract the two travel times $\Delta t(b_+)$ and $\Delta t(b_-)$ from each other to

obtain the time delay between the two images. To the leading orders of M/b and b/r_i , the result is found to be

$$\begin{aligned} \Delta^2 t_{\pm} &\equiv \Delta t(b_+) - \Delta t(b_-) \\ &= \left(-a_1 + b_1 v^2 + 2a_{01} \hat{q} \sqrt{1-v^2} \right) \frac{2\sqrt{1+\eta}}{v^3 \eta} \\ &\quad + \left[\left(\frac{2}{v} - \frac{1}{v^3} \right) a_1 - \frac{b_1}{v} + 2a_{01} \hat{q} \left(\frac{1}{v^2} - 1 \right)^{\frac{3}{2}} \right] \\ &\quad \times \ln \frac{\sqrt{1+\eta} - 1}{\sqrt{1+\eta} + 1} + \mathcal{O} \left(\beta M, \frac{b^3}{r_{s,d}^2}, \frac{M^2}{b} \right) \end{aligned} \quad (40)$$

where η is given by Eq. (34) or in terms of β as

$$\eta(\beta) = \frac{8r_s}{\beta^2(r_d + r_s)r_d} \left(-\frac{a_1}{2v^2} + \frac{b_1}{2} + \frac{a_{01} \hat{q} \sqrt{1-v^2}}{v^2} \right). \quad (41)$$

Formally, Eq. (40) agrees with the time delay for neutral particles (see Eq. (32) of Ref. [25]) except now the η contains contribution from electromagnetic interaction. In the limit

$$\eta \gg 1, \text{ i.e. } M/r_{d,s} \gg \beta_L^2 \sim \beta^2, \quad (42)$$

the two terms in Eq. (40) contribute similarly to the total time delay, and the result can be further simplified by large η expansion to be

$$\begin{aligned} \Delta^2 t_{\pm} &= \frac{4[(b_1 - a_1) + a_{01} \hat{q} \sqrt{1-v^2}]}{v\sqrt{\eta}} \\ &\quad + \mathcal{O} \left[M \left(\frac{r_{d,s}}{M} \beta^2 \right)^{\frac{3}{2}}, \beta M, \frac{b^3}{r_{s,d}^2}, \frac{M^2}{b} \right]. \end{aligned} \quad (43)$$

In the opposite limit, that is

$$\eta \ll 1, \quad M/r_{s,d} \ll \beta_L^2 \sim \beta^2, \quad (44)$$

the time delay becomes

$$\Delta^2 t_{\pm} = \frac{2(b_1 v^2 - a_1 + 2a_{01} \hat{q} \sqrt{1-v^2})}{v^3 \eta} + \mathcal{O} \left(M, \frac{b^3}{r_{s,d}^2} \right). \quad (45)$$

The effect of electromagnetic interaction on the time delay is slightly more tricky to analyze than in the case of the impact parameters and the apparent angles of the images. For both Eqs. (43) and (45), we see that at the lowest order, both the numerator and denominator will deviate from the neutral particle value in the same direction as \hat{q} deviates from zero (see Eq. (34) for η). Therefore we will have to go to one order higher to figure out the effect of the charge on $\Delta^2 t_{\pm}$. A small perturbative expansion shows that the deviation of the time delay $\Delta^2 t_{\pm}$ from the neutral particle value is given by $\tilde{c} \hat{q} Q$ with $\tilde{c} > 0$ when $|qQ|$ and β are both small (see Eq. (57) for its value in the RN spacetime). Therefore for small β , similar to the case of b_{\pm} , θ_{\pm} and μ_{\pm} , when $\text{sign}(qQ) = 1$

(or -1), $\Delta^2 t_{\pm}$ will be larger (or smaller) comparing to the neutral particle case. For larger $|qQ|$ and β , as we will see in Sec. IV A, the time delay between charged signal of both signs will be larger than that of neutral signals.

In summary, let us make the observation from Eqs. (23b), (30), (33) with (41), (35), (37) with (36), that the electromagnetic corrections to the gravitational values of all these quantities studied in this work depend on the relative size of the following quantities

$$\mathcal{O}(M), \quad \mathcal{O}(Qq/E). \quad (46)$$

Here for the order estimation purpose we have limited ourselves to relativistic signals so that v is close to 1, and without losing any generality we used $\mathcal{O}(b_1 - a_1) \approx \mathcal{O}(M)$ and $\mathcal{O}(-a_{01}) \approx \mathcal{O}(Q)$. If the latter in Eq. (46) is smaller than the former, then the gravitational contributions to these quantities are still larger, and otherwise the electromagnetic terms become dominate.

IV. APPLICATION TO THE CHARGED SPACETIMES

In this section we will apply the results found in Secs. II and III to some charged spacetime to demonstrate the effectiveness of the perturbative method, and to study in more details the effect of the electromagnetic interaction on the GEL observables.

A. The RN-type spacetimes

By RN-type spacetimes, here we include not only the well known RN BH spacetime but also any SSS spacetimes that has an exterior junction with the RN BH spacetimes, including charged fluid [46, 47], thin-shell wormhole [48], gravastar [49], compact star [50], anisotropic compact object [51, 52] and polytropic sphere [53] solutions. Because the signals studied in this work only travel in the weak field limit, the gravity and electric interaction they experience in these spacetimes are exact the same as in RN BH spacetimes carrying the same amount of charge.

The RN type spacetime is the simplest charge spacetime, asymptotically described by the following metric functions and electric potential

$$A(r) = \frac{1}{B(r)} = 1 - \frac{2M}{r} + \frac{Q^2}{r^2}, \quad A_0(r) = -\frac{Q}{r}. \quad (47)$$

Clear, they have particularly simple asymptotic expansion coefficients

$$a_0 = 1, \quad a_1 = -2M, \quad a_2 = Q^2, \quad a_n = 0 \quad (n \geq 3), \quad (48a)$$

$$b_0 = 1, \quad b_1 = 2M, \quad b_2 = 4M^2 - Q^2, \quad \dots, \quad (48b)$$

$$c_0 = 1, \quad c_n = 0 \quad (n \geq 1), \quad (48c)$$

$$a_{01} = -Q, \quad a_{0n} = 0 \quad (n \geq 1). \quad (48d)$$

Substituting these coefficients into (23) and then into (27), one finds the change of the angular coordinate in RN spacetime to the third order (second non-trivial order)

$$\begin{aligned} \Delta\phi_{\text{R}} = & \sum_{i=s,d} \left\{ \frac{\pi}{2} - \theta_i + c_i \left(1 + \frac{1}{v^2} - \frac{\hat{q}\hat{Q}\sqrt{1-v^2}}{v^2} \right) \frac{M}{b} \right. \\ & + \frac{1}{8} (\pi + 2s_i c_i - 2\theta_i) \left[3 \left(1 + \frac{4}{v^2} \right) \right. \\ & - \left. \left(1 + \frac{2}{v^2} \right) \hat{Q}^2 - \frac{12\hat{q}\hat{Q}\sqrt{1-v^2}}{v^2} \right. \\ & \left. \left. + 2 \left(\frac{1}{v^2} - 1 \right) \hat{q}^2 \hat{Q}^2 \right] \frac{M^2}{b^2} + \mathcal{O} \left(\frac{M^3}{b^3} \right) \right\}, \quad (49) \end{aligned}$$

where $\hat{Q} \equiv Q/M$ and the terms proportional to \hat{q}^n ($n \geq 1$) are the electromagnetic contributions. Setting \hat{q} to zero we recover the pure gravitational deflection in the RN spacetime (see Eq. (5.3) of Ref. [24]). In the large $r_{s,d}$ limit, θ_i can be expanded and then $\Delta\phi$ becomes

$$\begin{aligned} \Delta\phi_{\text{R}} = & \sum_{i=s,d} \left\{ \frac{\pi}{2} + \left(1 + \frac{1}{v^2} - \frac{\hat{q}\hat{Q}\sqrt{1-v^2}}{v^2} \right) \frac{M}{b} \right. \\ & + \frac{\pi}{8} \left[3 \left(1 + \frac{4}{v^2} \right) - \left(1 + \frac{2}{v^2} \right) \hat{Q}^2 \right. \\ & - \left. \frac{12\hat{q}\hat{Q}\sqrt{1-v^2}}{v^2} + 2 \left(\frac{1}{v^2} - 1 \right) \hat{q}^2 \hat{Q}^2 \right] \frac{M^2}{b^2} \\ & - \frac{b}{r_i} + \frac{1}{2} \left(\frac{1}{v^2} - 1 - \frac{\hat{q}\hat{Q}\sqrt{1-v^2}}{v^2} \right) \frac{b^2}{r_i^2} \frac{M}{b} \\ & \left. + \mathcal{O} \left(\frac{M^3}{b^3}, \frac{b^3}{r_i^3} \right) \right\} \quad (50) \end{aligned}$$

The finite distance effect in this formula is more transparent than in Eq. (49). It is seen that at the leading order of $b/r_{s,d}$, the finite distance of the source/detector would slightly decrease the deflection angle, as expected from the fact that the gravitational bending of the trajectories is always towards the lens. In the infinite distance limit, this is further simplified to

$$\begin{aligned} \Delta\phi_{\text{R}} = & \pi + 2 \left(1 + \frac{1}{v^2} - \frac{\hat{q}\hat{Q}\sqrt{1-v^2}}{v^2} \right) \frac{M}{b} \\ & + \frac{\pi}{4} \left[3 \left(1 + \frac{4}{v^2} \right) - \left(1 + \frac{2}{v^2} \right) \hat{Q}^2 \right. \\ & - \left. \frac{12\hat{q}\hat{Q}\sqrt{1-v^2}}{v^2} + 2 \left(\frac{1}{v^2} - 1 \right) \hat{q}^2 \hat{Q}^2 \right] \frac{M^2}{b^2} \\ & + \mathcal{O} \left(\frac{M^3}{b^3} \right) \quad (51) \end{aligned}$$

which agrees with Refs. [38, 39]. It is seen from Eq. (51) that the spacetime charge Q affects the deflection

gravitationally at the order $\mathcal{O}(M/b)^2$ but electrically at one order lower, i.e., at the order $\mathcal{O}(M/b)$. Also note that setting $M = 0$, Eq. (51) reduces to the pure relativistic electromagnetic deflection by a charge Q and agrees with known result in Ref. [54]. In this sense, setting $M = 0$ in Eq. (50) yields a relativistic Coulomb scattering deflection angle with finite distance effect of the source and detector taken into account.

The apparent angles of the images in the RN spacetime is obtained by substituting the coefficients (48) into Eq. (35). The result is

$$\theta_{\pm\text{R}} = b_{\pm\text{R}} \left[\frac{1}{r_d} + \left(\frac{-1}{v^2} + \frac{\hat{Q}\hat{q}\sqrt{1-v^2}}{v^2} \right) \frac{M}{r_d^2} \right] \quad (52)$$

where $b_{\pm\text{R}}$ is still given by Eq. (33) but η now takes the form

$$\eta_{\text{R}} = \frac{8(r_d + r_s)M}{\beta_L^2 r_d r_s} \left(\frac{1}{v^2} + 1 - \frac{\hat{Q}\hat{q}\sqrt{1-v^2}}{v^2} \right). \quad (53)$$

The magnification is still given by Eq. (39) with $u_\beta = \beta/\theta_{\text{E}}$ but now θ_{E} is updated to

$$\theta_{\text{E,R}} = \sqrt{\frac{2Mr_s}{r_d(r_s + r_d)} \left(\frac{1}{v^2} + 1 - \frac{\hat{Q}\hat{q}\sqrt{1-v^2}}{v^2} \right)}. \quad (54)$$

To compute the time delay in the RN spacetime, we can substitute the coefficients (48) into Eq. (40) and find

$$\begin{aligned} \Delta^2 t_{\pm\text{R}} = & \left(1 + v^2 - \hat{q}\hat{Q}\sqrt{1-v^2} \right) \frac{4M\sqrt{1+\eta}}{v^3\eta} \\ & + 2M \left[\frac{1}{v^3} - \frac{3}{v} - \hat{q}\hat{Q} \left(\frac{1}{v^2} - 1 \right)^{\frac{3}{2}} \right] \\ & \times \ln \frac{\sqrt{1+\eta} - 1}{\sqrt{1+\eta} + 1} + \mathcal{O} \left(\beta M, \frac{b^3}{r_{s,d}^2}, \frac{M^2}{b} \right) \quad (55) \end{aligned}$$

with η given in Eq. (53) or in terms of β

$$\eta_{\text{R}}(\beta) = \frac{8r_s M}{\beta^2 (r_d + r_s) r_d} \left(\frac{1}{v^2} + 1 - \frac{\hat{Q}\hat{q}\sqrt{1-v^2}}{v^2} \right). \quad (56)$$

From the illustration Fig. 2, we were clear that the flight times of charges with $\text{sign}(qQ) = 1$ (or $= -1$) from both sides will be larger (or smaller) than neutral signals, but the relative sizes of the time delays of the charged and neutral signal was not very transparent to us. In order to see how $\Delta^2 t_{\pm\text{R}}$ was affected by the electromagnetic interaction, one can expand Eq. (55) for small $\hat{q}\hat{Q}$ (note that η depends on $\hat{q}\hat{Q}$ too). Carrying out this expansion, the time delay at small $\hat{q}Q$ and small β becomes

$$\Delta^2 t_{\pm\text{R}}(\beta \rightarrow 0, \hat{q}\hat{Q} \rightarrow 0) = \beta \sqrt{\frac{2r_d(r_s + r_d)}{Mr_s}} \left[\frac{4M}{\sqrt{1+v^2}} \right]$$

$$+ \hat{q}Q \left(\frac{1-v^2}{1+v^2} \right)^{3/2} \Big] + \mathcal{O} \left[\beta^2, (\hat{q}\hat{Q})^2 \right]. \quad (57)$$

It is seen that at the leading order, for $\text{sign}(qQ) = 1$ (or $\text{sign}(qQ) = -1$), the time delay is actually larger (or smaller) comparing to neutral particles. For signals with larger β or $|qQ|$ however, numerical study show that time delay might depend on qQ differently (see Fig. 6 (b)).

To verify the correctness of the above results and illustrate more clearly the effect of the electromagnetic interaction, in below we will plot these variables as functions of b , β (or β_L) and Q . We assume that the deflection and GEL is caused by the Sgr A* SMBH, which carries a small charge. Although observationally the charge of the BH is not well constrained, theoretically there are at least three scales that can be used for reference. The first is related to the quasi-equilibrium of electrons and protons in the stellar atmosphere, which results in a small positive charge Q_{eq} of the astrophysical object [55, 56]

$$Q_{\text{eq}} \approx 100 \frac{M}{M_{\odot}} [\text{C}]. \quad (58)$$

If the charge of the BH is induced by the magnetic field B_{mag} around it, then its value should be around

$$Q_{\text{mag}} \approx 1.46 \times 10^2 \left(\frac{M}{M_{\odot}} \right)^2 \frac{B_{\text{mag}}}{10 [\text{G}]} [\text{C}], \quad (59)$$

where B_{mag} is typically of order 10 [G]. Note that for typical SMBHs having mass $M \gtrsim \mathcal{O}(10^6 M_{\odot})$ both these two charges are much smaller than the third scale of Q , i.e., the extreme RN spacetime limit Q_{extr}

$$Q_{\text{eq}} \ll Q_{\text{mag}} \ll Q_{\text{extr}} \approx 1.72 \times 10^{20} \frac{M}{M_{\odot}} [\text{C}]. \quad (60)$$

Observing all these, and to see the electromagnetic effect more clearly and adequately, in this work we will limit the charge Q to $\sqrt{Q_{\text{mag}} Q_{\text{extr}}} \approx 1.85 \times 10^6 Q_{\text{mag}} \approx Q_{\text{extr}} / (1.85 \times 10^6)$. Using the Sgr A* SMBH mass of $4.1 \times 10^6 M_{\odot}$, distance $r_d = 8.1$ [kpc] and assuming $r_s = r_d$, and for proton energy of 10^{19} [eV] (which then fixes its velocity), we plotted the deflection angle $\Delta\phi'_R$ defined as

$$\Delta\phi'_R = \Delta\phi_R - \pi - \theta_s - \theta_d \quad (61)$$

as functions of b and Q in Fig. 3, apparent angles $\theta_{\pm R}$, magnifications $\mu_{\pm R}$ and time delay $\Delta^2 t_{\pm R}$ as functions of β (or β_L) and Q in Figs. 4, 5 and 6 respectively.

In Fig. 3 (a), the deflection angle (61) with $\Delta\phi_R$ from Eq. (49) truncated to different orders of M/b , and the corresponding value obtained by direct numerical integration of Eq. (8) are plotted as functions of b . The truncation order is labeled by subscript n . It is seen that as the truncation order increases, the accuracy of the series result is also increasing. For very large b , from the inset we see that the contribution from each order also

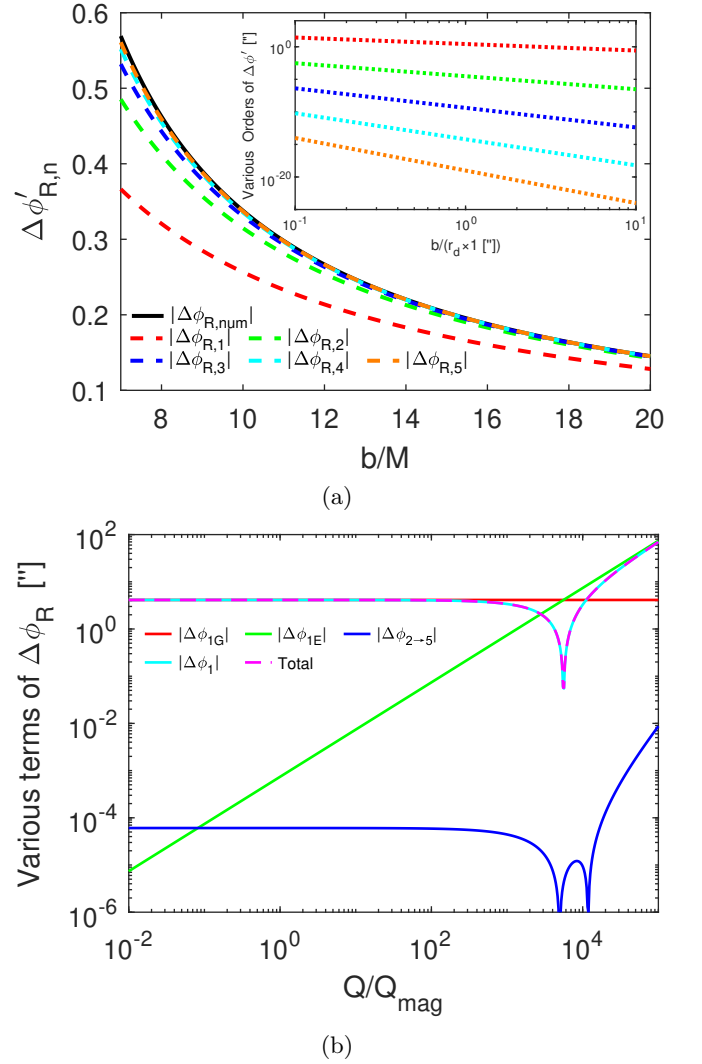


FIG. 3. The deflection angle $\Delta\phi'_R$ using Eq. (49). (a) Dash lines from bottom to top corresponds respectively to $\Delta\phi'_R$ truncated to $\mathcal{O}(M/b)^1$ to $\mathcal{O}(M/b)^5$ (note for clarity reason the 3rd-5th orders were not shown in Eq. (49) but the third order is given in Eq. (B3)). The solid line is the numerical integration result. Inset: from top to bottom the contributions from order $\mathcal{O}(M/b)^1$ to $\mathcal{O}(M/b)^5$ in Eqs. (49) for large b . Q is set to $2 \times 10^3 Q_{\text{mag}}$ in this subplot. (b) Various terms and orders of Eq. (49) as functions of Q . See text for details. b is set to $r_d \cdot 1$ ["] in this subplot.

decreases rapidly as the order increases, as expected from the expansions of $\Delta\phi_R$ given in Eqs. (50) or (51). Note that since in these plots the $b/r_{s,d}$ are all very small, the finite distance effect of the source/distance can not be distinguished in them. In order to see the relative contribution of the electromagnetic interaction to $\Delta\phi'_R$, in Fig. 3 (b) we plot as functions of Q the leading order contribution from the gravitational interaction $\Delta\phi_{1G}$ and electromagnetic interaction $\Delta\phi_{1E}$, which correspond respectively to the $(1 + \frac{1}{v^2}) \frac{M}{b}$ term and $-\frac{\hat{q}\hat{Q}\sqrt{1-v^2}}{v^2} \frac{M}{b}$ term in Eqs. (49), (50) or (51) (again, for the given b and $r_{s,d}$,

the finite distance effect can not be distinguished in the plot). The entire first order, $\Delta\phi_1$, the second to fifth order contribution, $\Delta\phi_{2\rightarrow 5}$, and the total $\Delta\phi'_R$ are also plotted. It is seen that the leading gravitational contribution dominates $\Delta\phi'_R$ when $Q \lesssim 5.58 \times 10^3 Q_{\text{mag}}$. This value is indeed determined by the comparison between $\Delta\phi_{1G}$ and $\Delta\phi_{1E}$ of Eq. (49), i.e., $\mathcal{O}\left(\frac{qQ}{E}\right) \approx \mathcal{O}(M)$, from which we obtain

$$Q \approx \frac{ME}{q} \approx 10^3 Q_{\text{mag}} \quad (62)$$

for the chosen M and signal energy E . If Q grows larger than this value, the electromagnetic contribution will be larger than the gravitational term, until Q reaches the value restricted by Eq. (25) at which point the perturbative method breaks down. Note that since in this figure the electromagnetic interaction between the proton and the central charge ($Q > 0$) is repulsive, when Q exceeds the value given by Eq. (62), the deflection angle $\Delta\phi'_R$ will change sign. That is, the traditional converging GEL effect will not happen and signals diverge away from the center, similar to lensing using concave lenses. In contrast, if the sign(qQ) < 0 , the converging lensing always happens, regardless the size of Q .

In Fig. 4, we plot the apparent angles $\theta_{\pm R}$ in Eq. (52) as functions of the source location β_L and lens charge Q . From Fig. 4 (a) we see that as β_L increases from 0 to about 10 ["], the θ_{-R} (or θ_{+R}) corresponding to the top (or bottom) trajectory in Fig. 1 increases (or decreases). For comparison, we also plotted for electrons and neutral particles with the same energy. For these three kinds of particles, the values of $\theta_{\pm R}$ at $\beta_L = 0$ are the corresponding Einstein ring size at the fixed Q , as specified by Eq. (54). More importantly, it is seen that the apparent angles of electrons from both the top and bottom trajectories from any fixed β_L are larger than those of neutral particles which in turn are larger than those of protons. This is in accord with the previous observation made after Eq. (36) that if sign(qQ) = 1 (or -1), the θ_{\pm} will be smaller (or larger) than neutral particle. This is a fundamental effect of the electrostatic interaction on the GEL image apparent angles, which is also reflected in Fig. 2. Fig. 4 (b) shows how these apparent angles evolve with the increase of Q . From this, it is clear that quantitatively as Q increases, the deviation of $\theta_{\pm R}$ of charged signal from that of neutral particle also increases.

In Fig. 5, the magnifications of the images as given in Eq. (39) with $\theta_{E,R}$ in Eq. (54) are plotted. It is seen from Fig. 5 (a) that both $\mu_{\pm R}$ decreases monotonically as β departs from zero. This is indeed expected from Eq. (39) because a larger β leads to larger u_β which decreases $\mu_{\pm R}$. On the other hand, it is seen from Fig. 5 (b) that as predicted by the analysis after Eq. (39), the larger Q leads to the smaller (or larger) $\theta_{E,R}$ and consequently smaller (or larger) magnifications for protons (or electrons) images.

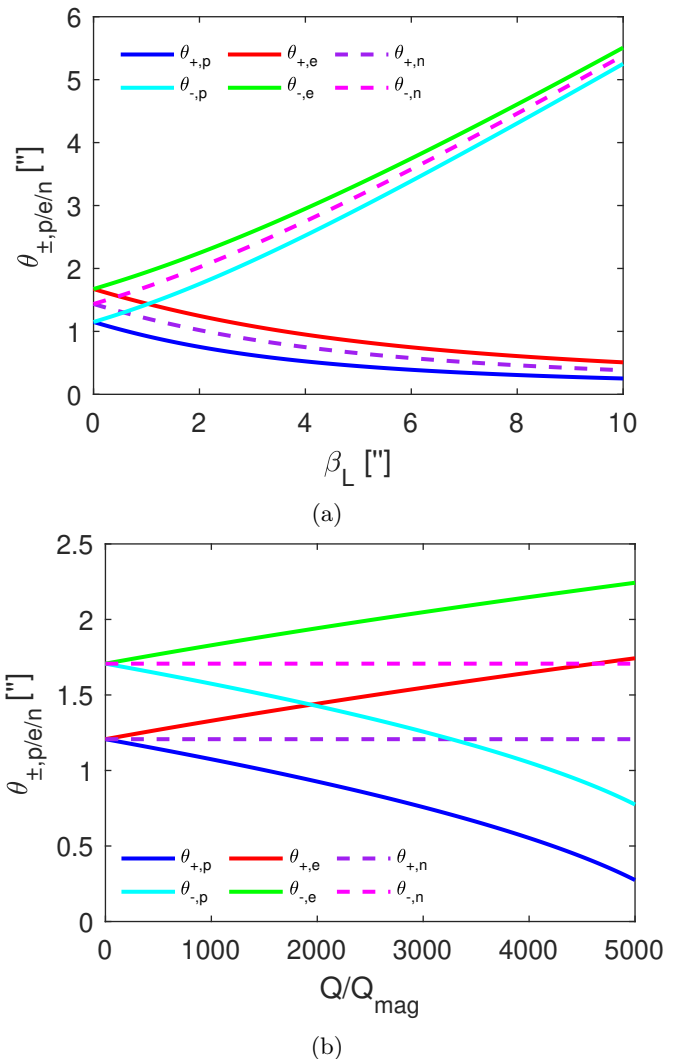


FIG. 4. The apparent angles $\theta_{\pm R}$ using Eq. (52). (a) The apparent angles' dependence on β_L for protons. For comparison, electrons with same energy and neutral particles with same velocity are also plotted. Q is set to $2.0 \times 10^3 Q_{\text{mag}}$ in this subplot. (b) The apparent angle as a function of Q . β_L is set to 1 ["] in this subplot.

Finally in Fig. 6, the time delay between the two images are plotted as a function of β_L and Q for UHE protons. To see the effect of particle charge (and only charge), we also plot the time delay of neutral particles and antiprotons. We chose to plot antiprotons rather than electrons because the time delay is sensitive to both velocity and energy of the signal, and only particles with the same mass can have both velocity and energy equal. It is seen from Fig. 6 (a) that for small β_L , the time delay for both the protons and antiprotons increase almost linearly as β_L increases. This can be understood from the case (43) and that $\eta \sim \beta_L^{-2}$ from the relation (34). As β_L grows larger to about ~ 6 ["], the condition (42) starts to break down and the time delay (55) deviate from Eq. (43). A simple numerical evaluation shows that

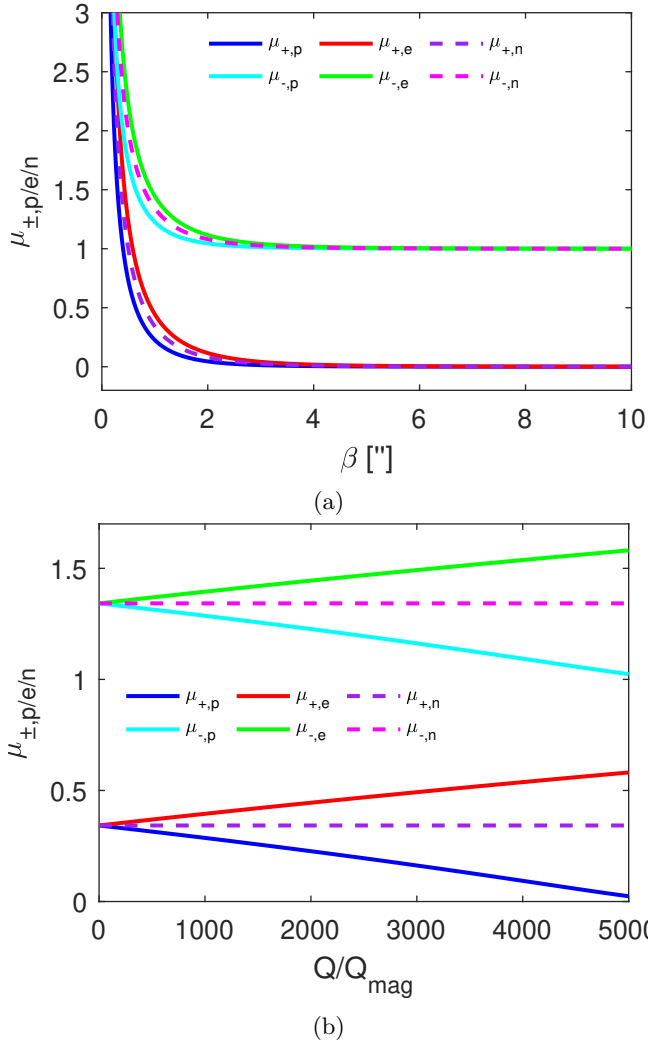


FIG. 5. The magnification $\mu_{\pm R}$ using Eq. (39). (a) Dependence of the magnification on β for protons. For comparison, electrons with same energy and neutral particles with same velocity are also plotted. Q is set to $2.0 \times 10^3 Q_{\text{mag}}$. (b) The magnification as a function of Q . β is set to 1 ["] in this subplot.

for the given range of β_L (less than 10 ["]), the opposite limit $\eta \ll 1$ still can not be reached and one should still use Eq. (55) to accurately describe the time delay for β_L from ~ 6 to 10 ["]. To distinguish the time delays for these signals, in the inset we plotted the difference of time delays of charged signals from neutral particles. It is seen that for the chosen $Q = 2 \times 10^3 Q_{\text{mag}}$ and the chosen range of β_L , signals with $\text{sign}(qQ) > 1$ have a time delay larger than $\text{sign}(qQ) < 1$ which in turn is larger than neutral particles time delay. For a large portion of the plotted β_L , their differences are both roughly a few seconds. This is much larger than typical observatory time resolutions such as neutrino or Gamma ray observatories, therefore allowing potential astrophysical applications, should the time delays of multi-messenger events be observed. In addition, we note that the above

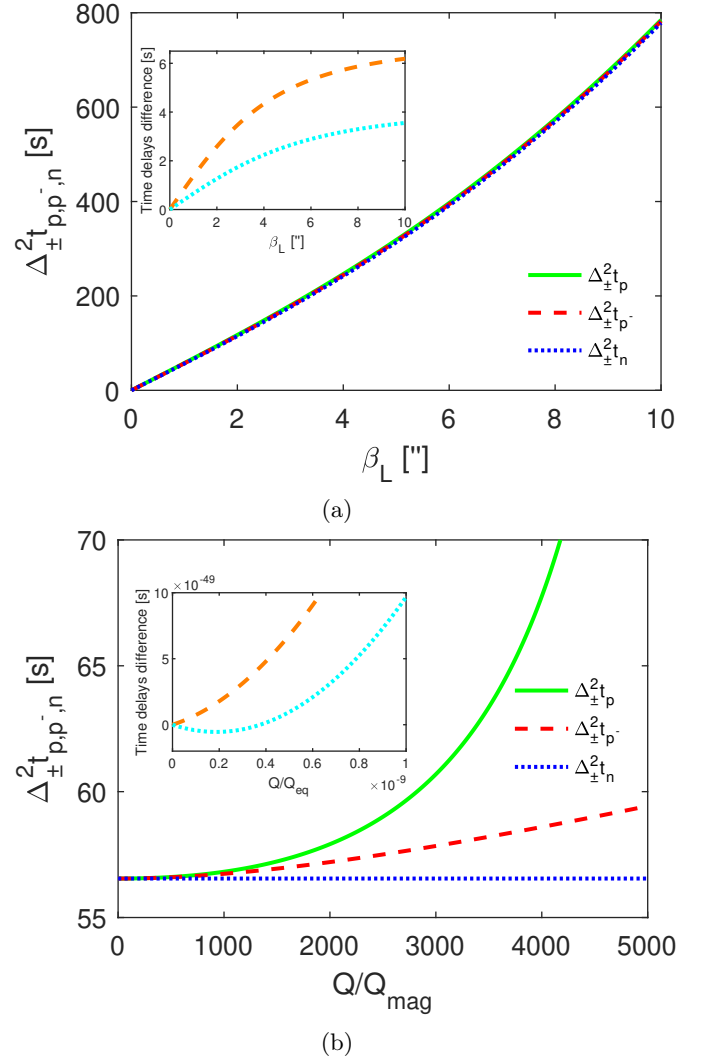


FIG. 6. The time delay $\Delta^2 t_{\pm R}$ using Eq. (55). (a) The dependence on β . All particles in this plot have the same velocity determined by 10^{19} [eV] protons. Inset: the differences between the proton time delay (orange) or antiproton time delay (cyan) against the neutral particles. Q was set to $2 \times 10^3 Q_{\text{mag}}$ in this subplot. (b) The dependence on Q for $\beta_L = 1$ ["]. Inset: dependence on Q when β is small ($\beta_L = 10^{-10}$ ["]).

ordering of the time delay is not a conflict to Eq. (57) because here the small $|qQ|$ condition is not satisfied.

In Fig. 6 (b), the effect of lens charge to the time delay is plotted. The inset shows the case that both β_L and $|qQ|$ are small. It is seen that in this case, as predicted by Eq. (57), the time delay for neutral particles is smaller than that of protons but larger than that of antiprotons with same velocity. When Q becomes larger than $4.0 \times 10^{-10} Q_{\text{eq}}$ however, both the protons and antiprotons have larger time delay than neutral particles. This is also the case for even larger Q and β_L , as shown in the main Fig. 6 (b). In this range of β_L and Q , the protons have larger time delay than antiprotons, and the time delay of neutral signals is the smallest.

Having gained a basic understanding of the relevant physics of the above quantities, we can now check how these observables can be used if they were measured. Among all parameters involved, for the signal particles, usually their charge q and energy E can be completely determined at the observatory. For the spacetime, we will assume that the lens mass M and its distance to the detector r_d can be fixed by other astrophysics means. For the GEL observables, usually the apparent angles θ_{+R} and θ_{-R} , as well as the ratio between the two magnification $r_\mu \equiv \mu_{-R}/\mu_{+R}$ can be measured. The time delay $\Delta^2 t_{\pm R}$ sometimes can also be obtained, depending on the observation conditions of the GEL system [57]. These observables indeed can be used to solve/constrain the lens/source parameters, such as the lens charge Q , source position β (or β_L) and source distance r_s , which are often not directly measurable.

Using Eq. (52) for the apparent angles of the image, Eq. (55) for the time delay, and the corresponding values of M , r_d for Sgr A* SMBH and q , E for UHE proton, we are indeed able to solve Q , β and r_s simultaneously. In Table I, we listed some typical values of $\theta_{\pm R}$ and $\Delta^2 t_{\pm R}$ and the solved values of β , Q and r_s . Unfortunately, due to the complexity of the above mentioned equations, the solution can only be expressed numerically.

B. GMGHS spacetime results

The GMGHS spacetime describing a charged dilaton spacetime is famous as a stringy BH spacetime. Deflection and lensing of neutral lightray in the weak field limit in this spacetime have been considered multiple times [58–60]. Recently, motion of charged test particle is also studied in this spacetime, concentrating on its inner-most stable circular orbit or BH shadow [61]. Here we consider the deflection and weak lensing of charged test particle in this spacetime for the first time (to our best knowledge).

The full GMGHS metric functions and four-potential are given by [42, 58]

$$\begin{aligned} A(r) &= \frac{1}{B(r)} = 1 - \frac{2M}{r}, \quad C(r) = r \left(r - \frac{Q^2 e^{-2\phi_0}}{M} \right), \\ A_0(r) &= -\frac{Q}{r}, \end{aligned} \quad (63)$$

where $\phi_0 \geq 0$ is the asymptotic value of the dilaton field. Apparently, the asymptotic coefficients are

$$a_0 = 1, \quad a_1 = -2M, \quad a_n = 0 \quad (n \geq 2), \quad (64a)$$

$$b_0 = 1, \quad b_1 = 2M, \quad b_2 = 4M^2, \quad \dots, \quad (64b)$$

$$c_0 = 1, \quad c_1 = -\frac{Q^2 e^{-2\phi_0}}{M}, \quad c_n = 0 \quad (n \geq 2), \quad (64c)$$

$$a_{01} = -Q, \quad a_{0n} = 0 \quad (n \geq 2). \quad (64d)$$

Substituting these into Eq. (23) and then (27), the

change of the angular coordinate becomes

$$\begin{aligned} \Delta\phi_G &= \sum_{i=s,d} \left\{ \frac{\pi}{2} - \theta_i + c_i \left(1 + \frac{1}{v^2} - \frac{\hat{q}\hat{Q}\sqrt{1-v^2}}{v^2} \right) \frac{M}{b} \right. \\ &\quad + \frac{1}{8} (\pi + 2s_i c_i - 2\theta_i) \left[3 \left(1 + \frac{4}{v^2} \right) \right. \\ &\quad \left. - e^{-2\phi_0} \hat{Q}^2 \left(1 + \frac{2}{v^2} \right) - \frac{e^{-4\phi_0} \hat{Q}^4}{4} \right. \\ &\quad \left. - 2 \left(6 - e^{-2\phi_0} \hat{Q}^2 \right) \frac{\hat{Q}\hat{q}\sqrt{1-v^2}}{v^2} \right. \\ &\quad \left. + 2 \left(\frac{1}{v^2} - 1 \right) \hat{q}^2 \hat{Q}^2 \right] \frac{M^2}{b^2} + \mathcal{O} \left(\frac{M^3}{b^3} \right) \right\} \quad (65) \end{aligned}$$

Comparing to the RN result, Eq. (49), we see from the $\mathcal{O}(M/b)^2$ order that the gravitational contribution of Q to $\Delta\phi$ now is tuned by the asymptotic dilaton factor $e^{-2\phi_0}$, which is inherited from the coefficient c_1 . On the contrary, the electromagnetic contribution of Q to $\Delta\phi$ appears only in one term in the second order of $\mathcal{O}(M/b)^2$, i.e., the $6 - e^{-2\phi_0} \hat{Q}^2$ term. Since usually we have $\hat{Q} \leq 1$, the effect of $e^{-2\phi_0}$ on the electromagnetic interaction is much weaker than that on the gravitational deflection. Although some works used a zero ϕ_0 [62, 63], indeed this is a variable not well constrained theoretically. When ϕ_0 is large, then it is seen that the gravitational contribution from the charge to $\Delta\phi$ is turned off while the electromagnetic one is still present, unaltered at the leading order.

Expanding Eq. (65) to the leading two orders of $b/r_{s,d}$, the finite distance $\Delta\phi$ that is parallel to Eq. (50) in the GMGHS case becomes

$$\begin{aligned} \Delta\phi_G &= \sum_{i=s,d} \left\{ \frac{\pi}{2} + \left(1 + \frac{1}{v^2} - \frac{\hat{q}\hat{Q}\sqrt{1-v^2}}{v^2} \right) \frac{M}{b} \right. \\ &\quad + \frac{\pi}{8} \left[3 \left(1 + \frac{4}{v^2} \right) - \left(1 + \frac{2}{v^2} \right) e^{-2\phi_0} \hat{Q}^2 \right. \\ &\quad \left. - \frac{e^{-4\phi_0} \hat{Q}^4}{4} - 2 \left(6 - e^{-2\phi_0} \hat{Q}^2 \right) \frac{\hat{q}\hat{Q}\sqrt{1-v^2}}{v^2} \right. \\ &\quad \left. + 2 \left(\frac{1}{v^2} - 1 \right) \hat{q}^2 \hat{Q}^2 \right] \frac{M^2}{b^2} - \frac{b}{r_i} \\ &\quad + \frac{1}{2} \left[\frac{1}{v^2} - 1 - \frac{\hat{q}\hat{Q}\sqrt{1-v^2}}{v^2} - e^{-2\phi_0} \hat{Q}^2 \right] \frac{b^2 M}{r_i^2} \\ &\quad \left. + \mathcal{O} \left(\frac{M^3}{b^3}, \frac{b^3}{r_i^3} \right) \right\}. \quad (66) \end{aligned}$$

The infinite $r_{s,d}$ result is given by the first three terms

$$\begin{aligned} \Delta\phi_G &= \pi + 2 \left(1 + \frac{1}{v^2} - \frac{\hat{q}\hat{Q}\sqrt{1-v^2}}{v^2} \right) \frac{M}{b} \\ &\quad + \frac{\pi}{4} \left[3 \left(1 + \frac{4}{v^2} \right) - \left(1 + \frac{2}{v^2} \right) e^{-2\phi_0} \hat{Q}^2 \right. \\ &\quad \left. - \frac{e^{-4\phi_0} \hat{Q}^4}{4} - 2 \left(6 - e^{-2\phi_0} \hat{Q}^2 \right) \frac{\hat{q}\hat{Q}\sqrt{1-v^2}}{2v^2} \right] \end{aligned}$$

Observables			Solved quantities		
θ_{+R} [']	θ_{-R} [']	$\Delta^2 t_{\pm R}$ [M]	β [']	Q [$10^{-9}M$]	r_s [r_d]
1.000	2.000	5.000	1.000	4.938	1.886
1.000	2.000	5.100	1.000	4.299	1.670
1.000	2.100	5.000	1.100	7.176	4.380
1.000	2.100	5.100	1.100	6.586	3.463
1.050	2.000	5.000	0.950	2.342	1.383
1.050	2.000	5.100	0.950	1.647	1.259
1.050	2.100	5.000	1.050	4.938	2.577
1.050	2.100	5.100	1.050	4.299	2.221

TABLE I. Constraining spacetime parameters and GEL configuration parameters using the observables. $M = 4.1 \times 10^6 M_\odot$ or 2.02×10^1 [second] after conversion using natural units, and $r_d = 8.1$ [kpc] for Sgr A* SMBH and $E = 10^{19}$ [eV] for proton are used. Unit of r_s is r_d .

$$+2 \left(\frac{1}{v^2} - 1 \right) \hat{q}^2 \hat{Q}^2 \left] \frac{M^2}{b^2} + \mathcal{O} \left(\frac{M^3}{b^3} \right) \quad (67)$$

For the apparent angles $\theta_{\pm G}$ of the GELED images in this spacetime, again substituting the expansions coefficients (64) into Eq. (35), we obtain the result

$$\theta_{\pm G} = b_{\pm G} \left[\frac{1}{r_d} + \left(\frac{-1}{v^2} + \frac{\hat{Q}e^{-2\phi_0}}{2} + \frac{\hat{Q}\hat{q}\sqrt{1-v^2}}{v^2} \right) \frac{M}{r_d^2} \right] \quad (68)$$

with the impact parameters $b_{\pm G}$ still given by Eq. (33) but with η_G taking the same form as η_R in Eq. (53) since both the RN and GMGHS spacetimes have the same a_1 , b_1 and a_{01} which fix η according to Eq. (34). For exactly the same reason, for the Einstein ring size $\theta_{E,G}$, the magnification $\mu_{\pm G}$ and the time delay $\Delta^2 t_{\pm G}$, which should be obtained by substituting a_1 , b_1 and a_{01} into Eqs. (36), (39) and (40) respectively, their formulas in the GMGHS spacetime are the same as in the RN-type spacetimes. In other words, these three quantities in the GMGHS spacetime are given by Eqs. (54), (39) with $u_\beta = \beta/\theta_{E,G}$ and (55) respectively.

C. Charged Horndeski theory result

Another spacetime that will be considered here is the charged Horndeski theory, whose metric functions and electric potential function are [43, 64, 65]

$$\begin{aligned} A(r) &= 1 - \frac{2M}{r} + \frac{Q^2}{4r^2} - \frac{Q^4}{192r^4}, \quad B(r) = \frac{1}{A(r)} \left(1 - \frac{Q^2}{8r^2} \right)^2, \\ C(r) &= r^2, \quad A_0(r) = -\frac{Q}{r} + \frac{Q^3}{24r^3}. \end{aligned} \quad (69)$$

Only when $Q^2 < 9M^2/2$, this describes a BH spacetime. The above have the following asymptotic expansions

$$\begin{aligned} a_0 &= 1, \quad a_1 = -2M, \quad a_2 = \frac{Q^2}{4}, \quad a_3 = 0, \\ a_4 &= -\frac{Q^2}{192}, \quad a_n = 0 \quad (n \geq 5), \end{aligned} \quad (70a)$$

$$b_0 = 1, \quad b_1 = 2M, \quad b_2 = 4M^2 - \frac{Q^2}{2}, \quad \dots, \quad (70b)$$

$$c_0 = 1, \quad c_n = 0 \quad (n \geq 1), \quad (70c)$$

$$a_{01} = -Q, \quad a_{02} = 0, \quad a_{03} = \frac{Q^3}{24}, \quad a_{0n} = 0 \quad (n \geq 4). \quad (70d)$$

Upto the second order, this set of asymptotic coefficients are very similar to the RN coefficients (48). The only differences, which appear in a_2 and b_2 (a_2 here is scaled by a factor of 1/4 and the Q^2 in b_2 is scaled by 1/2), are quantitative but not qualitative.

Substituting these coefficients into Eq. (23) and then (27), we obtain the change of the angular coordinate

$$\begin{aligned} \Delta\phi_H &= \sum_{i=s,d} \left\{ \frac{\pi}{2} - \theta_i + c_i \left(1 + \frac{1}{v^2} - \frac{\hat{q}\hat{Q}\sqrt{1-v^2}}{v^2} \right) \frac{M}{b} \right. \\ &\quad + \frac{1}{8} (\pi + 2s_i c_i - 2\theta_i) \left[3 \left(1 + \frac{4}{v^2} \right) - \left(1 + \frac{1}{v^2} \right) \frac{\hat{Q}^2}{2} \right. \\ &\quad \left. \left. - \frac{12\hat{q}\hat{Q}\sqrt{1-v^2}}{v^2} + 2 \left(\frac{1}{v^2} - 1 \right) \hat{q}^2 \hat{Q}^2 \right] \frac{M^2}{b^2} \right. \\ &\quad \left. + \mathcal{O} \left(\frac{M^3}{b^3} \right) \right\}. \end{aligned} \quad (71)$$

Comparing to the RN case (49), the difference of this $\Delta\phi$ is in the second order terms, caused by the numerical factor difference in a_2 and b_2 . Its small $b/r_{s,d}$ expansion to the second order is given by

$$\begin{aligned} \Delta\phi_H &= \sum_{i=s,d} \left\{ \frac{\pi}{2} + \left(1 + \frac{1}{v^2} - \frac{\hat{q}\hat{Q}\sqrt{1-v^2}}{v^2} \right) \frac{M}{b} \right. \\ &\quad + \frac{\pi}{8} \left[3 \left(1 + \frac{4}{v^2} \right) - \left(1 + \frac{1}{v^2} \right) \frac{\hat{Q}^2}{2} \right. \\ &\quad \left. \left. - \frac{12\hat{q}\hat{Q}\sqrt{1-v^2}}{v^2} + 2 \left(\frac{1}{v^2} - 1 \right) \hat{q}^2 \hat{Q}^2 \right] \frac{M^2}{b^2} \right. \\ &\quad \left. - \frac{b}{r_i} + \frac{1}{2} \left(\frac{1}{v^2} - 1 - \frac{\hat{q}\hat{Q}\sqrt{1-v^2}}{v^2} \right) \frac{b^2}{r_i^2} \frac{M}{b} \right. \end{aligned}$$

$$+\mathcal{O}\left(\frac{M^3}{b^3}, \frac{b^3}{r_i^3}\right)\}, \quad (72)$$

and the corresponding infinite distance result is simply

$$\begin{aligned} \Delta\phi_{\text{H}} = & \pi + 2 \left(1 + \frac{1}{v^2} - \frac{\hat{q}\hat{Q}\sqrt{1-v^2}}{v^2} \right) \frac{M}{b} \\ & + \frac{\pi}{4} \left[3 \left(1 + \frac{4}{v^2} \right) - \left(1 + \frac{1}{v^2} \right) \frac{\hat{Q}^2}{2} \right. \\ & \left. - \frac{12\hat{q}\hat{Q}\sqrt{1-v^2}}{v^2} + 2 \left(\frac{1}{v^2} - 1 \right) \hat{q}^2 \hat{Q}^2 \right] \frac{M^2}{b^2} \\ & + \mathcal{O}\left(\frac{M^3}{b^3}, \frac{b^3}{r_i^3}\right). \end{aligned} \quad (73)$$

Setting $\hat{q} = 0$ and taking $v = 1$, this further reduces to the deflection of chargeless null rays, and it agrees with Eq. (3.1) of Ref. [65].

For GEL by the Horndeski black hole, the impact parameters $b_{\pm\text{H}}$ and other observables including apparent angles $\theta_{\pm\text{H}}$, magnifications $\mu_{\pm\text{H}}$ and time delay $\Delta^2 t_{\pm\text{H}}$, can be obtained respectively from Eqs. (33), (35), (39), (40). One important thing to notice is that these equations are all given to the leading order(s) and therefore are determined by the expansion coefficients up to order a_1 , b_1 , c_1 and a_{01} of the metric functions and four-potential. Since to this order, coefficients for the Horndeski BH as given in Eq. (70) have the same form as in the RN spacetime given in Eq. (48), the above mentioned quantities in the Horndeski case would also take the same form as in the RN case. In other words, $b_{\pm\text{H}}$ is still given by Eq. (33) with (53), $\theta_{\pm\text{H}}$ by Eq. (52), $\mu_{\pm\text{H}}$ by Eq. (39) with (54) and finally $\Delta^2 t_{\pm\text{H}}$ by Eq. (55). If one is interested in the higher order difference between these quantities in the Horndeski and RN spacetimes, higher orders have to be pursued in the general formulas for these quantities. Although this is technically possible, we will not continue along this direction because it seems not much more physics can be gained.

V. CONCLUSIONS AND DISCUSSIONS

In this work, we considered using a perturbative approach the deflection angle and dual lensing of charge signals due to the gravitational and electromagnetic interactions in the weak field limit in general charged SSS spacetime. Our method can address not only the bending and GEL of null but also timelike particles, not only charged but also neutral particles. Moreover, the finite distance effect of the source/observer is also taken into account, which allows us to solve an exact lensing equation.

It is found in Eqs. (23b) and (29) that the change of the angular coordinate $\Delta\phi$ receives an electromagnetic modification from the first non-trivial order. Depending on the sign of qQ , this electromagnetic modification might increase (for $\text{sign}(qQ) = -1$) or decrease (for

$\text{sign}(qQ) = 1$) the deflection angle by the amount determined by the size of qQ/E . In GEL, the extra electromagnetic interaction will decrease (or increase) the impact parameters and apparent angles of both images and the Einstein ring size if $\text{sign}(qQ) = 1$ (or $\text{sign}(qQ) = -1$), according to Eqs. (33) to (36). This is intuitively understandable from the fact that the same (or different) signs of q and Q will cause an extra repulsion (or attraction) between the lens and the signal and therefore the impact parameter has to adjust oppositely in order for the signals from the same source to reach the same observer.

For the total travel time, for the same reasoning as in the case of deflection angle, $\text{sign}(qQ) = 1$ (or $\text{sign}(qQ) = -1$) will decrease (or increase) Δt for signals from both sides. The more interesting quantity here is effect of electromagnetic interaction on the time delay between the two images, which is the difference between two decreased or increased total travel times. It is found that for extremely small β and $|qQ|$, comparing to neutral particles, the positive (or negative) $\text{sign}(qQ)$ actually will increase (or decrease) the time delay. For larger qQ or β however, time delay of both positive and negative charges will be larger than that of the neutral particle with same velocity.

The application of the results to three charged spacetimes in Sec. IV, especially to the RN spacetime, confirms the above conclusions drawn according to the results in general SSS spacetime. The charge of the spacetime we numerically considered is much smaller than its mass, and the charged particles are mainly the UHE protons in cosmic rays, although sometimes for comparison purpose electrons and neutral particles are also considered. We also applied the results to the GHGMS and charged Horndeski spacetimes.

ACKNOWLEDGMENTS

X. Xu and T. Jiang thank Mr. Zonghai Li and Mr. Ruizhe Liang for valuable discussions. This work is supported by the NNSF China 11504276 and MOST China 2014GB109004.

Appendix A: Integral formulas

When integrating Eqs. (14) and (17) with Eq. (23), and Eq. (24), we need to compute integrals of the following form

$$I_n(\theta_i) = \int_{\sin\theta}^1 \frac{u^n}{\sqrt{1-u^2}} du \quad (n = -2, -1, \dots). \quad (\text{A1})$$

This integral can be carried out using a change of variables $u = \sin\xi$ to find an elementary expression

$$I_n(\theta_i) = \int_{\theta}^{\pi/2} \sin^n \xi d\xi$$

$$= \begin{cases} \cot \theta_i, & n = -2, \\ \ln [\cot (\frac{\theta_i}{2})], & n = -1, \\ \frac{(n-1)!!}{n!!} \left(\frac{\pi}{2} - \theta_i + \cos \theta_i \sum_{j=1}^{\lfloor \frac{n}{2} \rfloor} \frac{(2j-2)!!}{(2j-1)!!} \sin^{2j-1} \theta_i \right), & n = 0, 2, \dots, \\ \frac{(n-1)!!}{n!!} \cos \theta_i \left(1 + \sum_{j=1}^{\lfloor \frac{n}{2} \rfloor} \frac{(2j-1)!!}{(2j)!!} \sin^{2j} \theta_i \right), & n = 1, 3, \dots. \end{cases} \quad (\text{A2})$$

In the $\theta = 0$ limit, i.e., the infinite source/detector distance limit, I_n for non-negative n can be further simplified

$$I_n(0) = \frac{(n-1)!!}{n!!} \begin{cases} \frac{\pi}{2}, & n = 0, 2, \dots, \\ 1, & n = 1, 3, \dots. \end{cases} \quad (\text{A3})$$

To present the effect of finite source/detector distance to the deflection angle and time delay in a more transparent way, we will need the expansion of the first few $I_n(\theta_i)$ in the limit of small b/r_i and M/b . They can be obtained by expanding θ_i in Eq. (16) for any given b and find

$$I_{-2} = \frac{r_i}{b} - \frac{b}{2r_i} - \left(\frac{a_1}{2v^2} - \frac{c_1}{2} - \frac{a_{01}\hat{q}\sqrt{1-v^2}}{v^2} \right) \frac{1}{b} + \mathcal{O} \left(\frac{b^2}{r_i^2}, \frac{M^2}{b^2} \right), \quad (\text{A4a})$$

$$I_{-1} = -\ln \left(\frac{b}{2r_i} \right) - \left(\frac{a_1}{2v^2} - \frac{c_1}{2} - \frac{a_{01}\hat{q}\sqrt{1-v^2}}{v^2} \right) \frac{b}{r_i} \frac{1}{b} + \mathcal{O} \left(\frac{b^2}{r_i^2}, \frac{M^2}{b^2} \right), \quad (\text{A4b})$$

$$I_0 = \frac{\pi}{2} - \frac{b}{r_i} - \left(\frac{a_1}{2v^2} - \frac{c_1}{2} - \frac{a_{01}\hat{q}\sqrt{1-v^2}}{v^2} \right) \frac{b}{r_i^2} + \mathcal{O} \left(\frac{b^3}{r_i^3}, \frac{M^2}{b^2} \right), \quad (\text{A4c})$$

$$I_1 = 1 - \frac{b^2}{2r_i^2} + \mathcal{O} \left(\frac{b^3}{r_i^3}, \frac{M^2}{b^2} \right), \quad (\text{A4d})$$

$$I_2 = \frac{\pi}{4} + \mathcal{O} \left(\frac{b^3}{r_i^3}, \frac{M^2}{b^2} \right). \quad (\text{A4e})$$

Appendix B: Integral formulas

The coefficients y_n and z_n in Eqs. (27) and (28) essentially determines the results for the change of angular coordinate $\Delta\phi$ and time coordinate Δt . Besides those given in Eqs. (23) and (24), here we list one more orders of them. That is,

$$y_3 = \left(\frac{1}{16v^6} - \frac{3}{4v^4} - \frac{3}{2v^2} \right) a_1^3$$

$$\begin{aligned} & + \left(\frac{3}{16v^4} + \frac{3}{4v^2} \right) a_1^2 (b_1 + 2c_1) + \left[\frac{3b_1(b_1 - 4c_1)}{16v^2} \right. \\ & + \left. \left(\frac{1}{4v^4} + \frac{1}{v^2} \right) 3a_2 - \frac{3(b_2 + 2c_2)}{4v^2} \right] a_1 \\ & + \left[\frac{b_1(b_1 - 2c_1)}{16} + \left(-\frac{3a_2}{4v^2} - \frac{b_2}{4} + \frac{c_2}{2} \right) \right] b_1 \\ & + \left(-\frac{3a_2}{2v^2} + \frac{b_2}{2} \right) c_1 - \frac{3a_3}{2v^2} + \frac{b_3}{2} + c_3 \\ & - a_{01}\hat{q}\sqrt{1-v^2} \left\{ \left(\frac{3}{8v^6} - \frac{3}{v^4} - \frac{3}{v^2} \right) a_1^2 \right. \\ & + \left. \left(\frac{3}{4v^4} + \frac{3}{2v^2} \right) [a_1(b_1 + 2c_1) + 2a_2] \right. \\ & + \left. \frac{3}{8v^2} [b_1(b_1 - 4c_1) - 4b_2 - 8c_2] \right\} \\ & - 3 \left[a_1 \left(\frac{1}{2v^4} + \frac{1}{v^2} \right) - \frac{b_1 + 2c_1}{2v^2} \right] a_{02}\hat{q}\sqrt{1-v^2} \\ & + \frac{3a_{03}\hat{q}\sqrt{1-v^2}}{v^2} + 3a_{01}\hat{q}^2(1-v^2) \\ & \times \left\{ a_1 a_{01} \left(\frac{1}{4v^6} - \frac{5}{4v^4} - \frac{1}{2v^2} \right) \right. \\ & + \left. \left(\frac{1}{v^4} + \frac{1}{v^2} \right) (a_{01}[b_1 + 2c_1] + 4a_{02}) \right\} \\ & - \left(\frac{1}{2v^6} - \frac{3}{2v^4} \right) a_{01}^3 \hat{q}^3 (1-v^2)^{3/2}, \quad (\text{B1}) \end{aligned}$$

and

$$\begin{aligned} z_2 = & - \left(\frac{1}{16v^7} - \frac{3}{8v^5} + \frac{3}{2v^3} + \frac{1}{v} \right) a_1^3 \\ & - \left(\frac{1}{16v^5} - \frac{1}{2v^3} - \frac{1}{2v} \right) a_1^2 (b_1 + 2c_1) \\ & + \left[\left(-\frac{1}{4v^5} + \frac{2}{v^3} + \frac{2}{v} \right) a_2 \right. \\ & + \left. \left(\frac{1}{16v^3} + \frac{1}{8v} \right) b_1 (b_1 - 4c_1) \right. \\ & - \left. \left(\frac{1}{4v^3} + \frac{1}{2v} \right) (b_2 + 2c_2) \right] a_1 + \frac{b_1^3}{16v} - \frac{b_1^2 c_1}{8v} \\ & - \left[\left(\frac{1}{4v^3} + \frac{1}{2v} \right) a_2 + \frac{1}{4v} (b_2 - 2c_2) \right] b_1 \\ & + \left[\left(-\frac{1}{2v^3} - \frac{1}{v} \right) a_2 + \frac{b_2}{2v} \right] c_1 \\ & - \left(\frac{1}{2v^3} + \frac{1}{v} \right) a_3 + \frac{1}{2v} (b_3 + 2c_3) \\ & + \frac{a_{01}\hat{q}\sqrt{1-v^2}}{v} \left\{ \left(\frac{3}{8v^6} - \frac{13}{8v^4} + \frac{4}{v^2} + 1 \right) a_1^2 \right. \\ & + \left. \left(\frac{1}{4v^4} - \frac{5}{4v^2} - \frac{1}{2} \right) [a_1(b_1 + 2c_1) + 2a_2] \right. \\ & - \left. \left(\frac{1}{8v^2} + \frac{1}{8} \right) [b_1(b_1 - 4c_1) - 4b_2 - 8c_2] \right\} \end{aligned}$$

$$\begin{aligned}
& + \left[\left(\frac{1}{2v^4} - \frac{5}{2v^2} - 1 \right) a_1 + \left(\frac{1}{v^2} + 1 \right) (b_1 + 2c_1) \right] \\
& \times \frac{a_{02} \hat{q} \sqrt{1-v^2}}{2v} + \left(\frac{1}{v^2} + 1 \right) \frac{a_{03} \hat{q} \sqrt{1-v^2}}{v} \\
& + a_{01} \hat{q}^2 (1-v^2) \left[\left(-\frac{3}{4v^7} + \frac{9}{4v^5} - \frac{3}{v^3} \right) a_1 a_{01} \right. \\
& \left. - \left(\frac{1}{4v^5} - \frac{3}{4v^3} \right) (a_{01} (b_1 + 2c_1) + 4a_{02}) \right] \\
& + (1-v^2)^2 \frac{a_{01}^3 \hat{q}^3 (1-v^2)^{3/2}}{2v^7}. \tag{B2}
\end{aligned}$$

In RN spacetime, the y_3 becomes

$$\begin{aligned}
y_3 = M^3 & \left\{ \frac{1}{2} \left(5 + \frac{45}{v^2} + \frac{15}{v^4} - \frac{1}{v^6} \right) \right. \\
& \left. + 3 \left(-\frac{15}{2v^2} - \frac{5}{v^4} + \frac{1}{2v^6} \right) \hat{q} \hat{Q} \sqrt{1-v^2} \right.
\end{aligned}$$

$$\begin{aligned}
& + 3 \left[-\frac{1}{2} - \frac{3}{v^2} - \frac{1}{2v^4} \right. \\
& \left. + \left(\frac{3}{2v^2} + \frac{3}{v^4} - \frac{1}{2v^6} \right) \hat{q}^2 (1-v^2) \right] \hat{Q}^2 \\
& + \left[\left(\frac{9}{2v^2} + \frac{3}{2v^4} \right) \hat{q} \sqrt{1-v^2} \right. \\
& \left. + \left(-\frac{3}{2v^4} + \frac{1}{2v^6} \right) \hat{q}^3 (1-v^2)^{3/2} \right] \hat{Q}^3 \Big\} \tag{B3}
\end{aligned}$$

It is seen that there is a term proportional to $\hat{q} \sqrt{1-v^2} \hat{Q}^3$. This indeed is a gravitational-electromagnetic coupling term, with a factor $\hat{q} \sqrt{1-v^2} \hat{Q}$ due to electromagnetic interaction and another factor \hat{Q}^2 due to gravitational contribution from the lens charge.

-
- [1] F. W. Dyson, A. S. Eddington and C. Davidson, Phil. Trans. Roy. Soc. Lond. A **220**, 291 (1920).
- [2] K. Sharon and T. L. Johnson, Astrophys. J. **800**, no. 2, L26 (2015)
- [3] C. Y. Peng, C. D. Impey, H. W. Rix, C. S. Kochanek, C. R. Keeton, E. E. Falco, J. Lehar and B. A. McLeod, Astrophys. J. **649**, 616 (2006) [astro-ph/0603248].
- [4] M. Bartelmann and P. Schneider, Phys. Rept. **340**, 291 (2001) [astro-ph/9912508].
- [5] P. A. R. Ade *et al.* [Planck Collaboration], Astron. Astrophys. **594**, A15 (2016)
- [6] A. Refregier, Ann. Rev. Astron. Astrophys. **41**, 645 (2003) [astro-ph/0307212].
- [7] A. Lewis and A. Challinor, Phys. Rept. **429**, 1 (2006) [astro-ph/0601594].
- [8] R. B. Metcalf and P. Madau, Astrophys. J. **563**, 9 (2001) [astro-ph/0108224].
- [9] H. Hoekstra and B. Jain, Ann. Rev. Nucl. Part. Sci. **58**, 99 (2008)
- [10] K. Hirata *et al.* [Kamiokande-II Collaboration], Phys. Rev. Lett. **58**, 1490 (1987).
- [11] R. M. Bionta *et al.*, Phys. Rev. Lett. **58**, 1494 (1987).
- [12] M. G. Aartsen *et al.* [IceCube and Fermi-LAT and MAGIC and AGILE and ASAS-SN and HAWC and H.E.S.S. and INTEGRAL and Kanata and Kiso and Kapteyn and Liverpool Telescope and Subaru and Swift NuSTAR and VERITAS and VLA/17B-403 Collaborations], Science **361**, no. 6398, eaat1378 (2018)
- [13] M. G. Aartsen *et al.* [IceCube Collaboration], Science **361**, no. 6398, 147 (2018)
- [14] B. P. Abbott *et al.* [LIGO Scientific and Virgo Collaborations], Phys. Rev. Lett. **116**, no. 6, 061102 (2016) doi:10.1103/PhysRevLett.116.061102 [arXiv:1602.03837 [gr-qc]].
- [15] B. P. Abbott *et al.* [LIGO Scientific and Virgo Collaborations], Phys. Rev. Lett. **116**, no. 24, 241103 (2016) doi:10.1103/PhysRevLett.116.241103 [arXiv:1606.04855 [gr-qc]].
- [16] B. P. Abbott *et al.* [LIGO Scientific and Virgo Collaborations], Phys. Rev. Lett. **119**, no. 14, 141101 (2017) doi:10.1103/PhysRevLett.119.141101 [arXiv:1709.09660 [gr-qc]].
- [17] B. P. Abbott *et al.* [LIGO Scientific and Virgo Collaborations], Phys. Rev. Lett. **119**, no. 16, 161101 (2017) doi:10.1103/PhysRevLett.119.161101 [arXiv:1710.05832 [gr-qc]].
- [18] B. P. Abbott *et al.* [LIGO Scientific and Virgo and Fermi-GBM and INTEGRAL Collaborations], Astrophys. J. **848**, no. 2, L13 (2017) doi:10.3847/2041-8213/aa920c [arXiv:1710.05834 [astro-ph.HE]].
- [19] A. Letessier-Selvon and T. Stanev, Rev. Mod. Phys. **83**, 907-942 (2011) doi:10.1103/RevModPhys.83.907 [arXiv:1103.0031 [astro-ph.HE]].
- [20] R. Alves Batista, J. Biteau, M. Bustamante, K. Dolag, R. Engel, K. Fang, K. H. Kampert, D. Kostunin, M. Mostafa and K. Murase, *et al.* Front. Astron. Space Sci. **6**, 23 (2019) doi:10.3389/fspas.2019.00023 [arXiv:1903.06714 [astro-ph.HE]].
- [21] X. Liu, J. Jia and N. Yang, Class. Quant. Grav. **33**, no.17, 175014 (2016) doi:10.1088/0264-9381/33/17/175014 [arXiv:1512.04037 [gr-qc]].
- [22] G. He and W. Lin, Class. Quant. Grav. **33**, no. 9, 095007 (2016) Addendum: [Class. Quant. Grav. **34**, no. 2, 029401 (2017)] doi:10.1088/0264-9381/33/9/095007, 10.1088/1361-6382/aa5203 [arXiv:2007.08754 [gr-qc]].
- [23] X. Pang and J. Jia, Class. Quant. Grav. **36**, no.6, 065012 (2019) doi:10.1088/1361-6382/ab0512 [arXiv:1806.04719 [gr-qc]].
- [24] K. Huang and J. Jia, JCAP **08**, 016 (2020) doi:10.1088/1475-7516/2020/08/016 [arXiv:2003.08250 [gr-qc]].
- [25] H. Liu and J. Jia, [arXiv:2006.03542 [gr-qc]].
- [26] H. Liu and J. Jia, Eur. Phys. J. C **80**, no.10, 932 (2020) doi:10.1140/epjc/s10052-020-08496-5 [arXiv:2006.11125 [gr-qc]].
- [27] Y. Duan, W. Hu, K. Huang and J. Jia, Class. Quant. Grav. **37**, no.14, 145004 (2020) doi:10.1088/1361-6382/ab852c [arXiv:2001.03777 [gr-qc]].

- [28] J. Jia, Eur. Phys. J. C **80**, no.3, 242 (2020) doi:10.1140/epjc/s10052-020-7796-y [arXiv:2001.02038 [gr-qc]].
- [29] G. He, X. Zhou, Z. Feng, X. Mu, H. Wang, W. Li, C. Pan and W. Lin, Eur. Phys. J. C **80**, no. 9, 835 (2020). doi:10.1140/epjc/s10052-020-8382-z
- [30] G. Crisnejo and E. Gallo, Phys. Rev. D **97**, no.12, 124016 (2018) doi:10.1103/PhysRevD.97.124016 [arXiv:1804.05473 [gr-qc]].
- [31] K. Jusufi, Phys. Rev. D **98**, no. 6, 064017 (2018) doi:10.1103/PhysRevD.98.064017 [arXiv:1806.01256 [gr-qc]].
- [32] K. Jusufi, [arXiv:1906.12186 [gr-qc]].
- [33] Z. Li, G. He and T. Zhou, Phys. Rev. D **101**, no. 4, 044001 (2020) doi:10.1103/PhysRevD.101.044001 [arXiv:1908.01647 [gr-qc]].
- [34] G. Crisnejo, E. Gallo and K. Jusufi, Phys. Rev. D **100**, no.10, 104045 (2019) doi:10.1103/PhysRevD.100.104045 [arXiv:1910.02030 [gr-qc]].
- [35] W. Javed, R. Babar and A. Övgün, Phys. Rev. D **100**, no. 10, 104032 (2019) doi:10.1103/PhysRevD.100.104032 [arXiv:1910.11697 [gr-qc]].
- [36] Z. Li and J. Jia, Eur. Phys. J. C **80**, no.2, 157 (2020) doi:10.1140/epjc/s10052-020-7665-8 [arXiv:1912.05194 [gr-qc]].
- [37] Z. Li and A. Övgün, Phys. Rev. D **101**, no. 2, 024040 (2020) doi:10.1103/PhysRevD.101.024040, 10.20944/preprints201911.0195.v1 [arXiv:2001.02074 [gr-qc]].
- [38] G. Crisnejo, E. Gallo and J. R. Villanueva, Phys. Rev. D **100**, no.4, 044006 (2019) doi:10.1103/PhysRevD.100.044006 [arXiv:1905.02125 [gr-qc]].
- [39] Z. Li, Y. Duan and J. Jia, [arXiv:2012.14226 [gr-qc]].
- [40] G. W. Gibbons, Nucl. Phys. B **207**, 337-349 (1982) doi:10.1016/0550-3213(82)90170-5
- [41] G. W. Gibbons and K. i. Maeda, Nucl. Phys. B **298**, 741-775 (1988) doi:10.1016/0550-3213(88)90006-5
- [42] D. Garfinkle, G. T. Horowitz and A. Strominger, Phys. Rev. D **43**, 3140 (1991) [erratum: Phys. Rev. D **45**, 3888 (1992)] doi:10.1103/PhysRevD.43.3140
- [43] A. Cisterna and C. Erices, Phys. Rev. D **89**, 084038 (2014) doi:10.1103/PhysRevD.89.084038 [arXiv:1401.4479 [gr-qc]].
- [44] F. Rohrlich, *Classical Charged Particles*, World Scientific, 2007, 3rd ediction
- [45] P. Schneider, C. S. Kochanek and J. Wambsganss, Saas-Fee Advanced Courses **33**, pp.1-553 (2006)
- [46] P. Anninos and T. Rothman, Phys. Rev. D **65**, 024003 (2002) doi:10.1103/PhysRevD.65.024003 [gr-qc/0108082].
- [47] B. V. Ivanov, Phys. Rev. D **65**, 104001 (2002) doi:10.1103/PhysRevD.65.104001 [gr-qc/0203070].
- [48] E. F. Eiroa and G. E. Romero, Gen. Rel. Grav. **36**, 651 (2004) doi:10.1023/B:GERG.0000016916.79221.24 [gr-qc/0303093].
- [49] D. Horvat, S. Ilijic and A. Marunovic, Class. Quant. Grav. **26**, 025003 (2009) doi:10.1088/0264-9381/26/2/025003 [arXiv:0807.2051 [gr-qc]].
- [50] S. K. Maurya, Y. K. Gupta, S. Ray and S. R. Chowdhury, Eur. Phys. J. C **75**, no. 8, 389 (2015). doi:10.1140/epjc/s10052-015-3615-2
- [51] E. Morales and F. Tello-Ortiz, Eur. Phys. J. C **78**, no. 8, 618 (2018) doi:10.1140/epjc/s10052-018-6102-8 [arXiv:1805.00592 [gr-qc]].
- [52] M. Sharif and S. Sadiq, Eur. Phys. J. C **78**, no. 5, 410 (2018) doi:10.1140/epjc/s10052-018-5894-x [arXiv:1804.09616 [gr-qc]].
- [53] J. D. V. Arbañil, J. P. S. Lemos and V. T. Zanchin, Phys. Rev. D **88**, 084023 (2013) doi:10.1103/PhysRevD.88.084023 [arXiv:1309.4470 [gr-qc]].
- [54] T. Padmanabhan, *Gravitation: Foundations and Frontiers*, Cambridge University Press (2010), Eq. (2.94)
- [55] Eddington, A. S., *The Internal Constitution of the Stars* (Cambridge University Press, 1926)
- [56] Bally J., Harrison E. R., Astrophysical J. **220**, 743 (1978).
- [57] C.S. Kochanek, E.E. Falco, C. Impey, J. Lehar, B. McLeod, H.-W. Rix, <https://lweb.cfa.harvard.edu/castles/>
- [58] A. Bhadra, Phys. Rev. D **67**, 103009 (2003) doi:10.1103/PhysRevD.67.103009 [arXiv:gr-qc/0306016 [gr-qc]].
- [59] C. R. Keeton and A. O. Petters, Phys. Rev. D **72**, 104006 (2005) doi:10.1103/PhysRevD.72.104006 [arXiv:gr-qc/0511019 [gr-qc]].
- [60] A. Övgün, G. Gylchev and K. Jusufi, Annals Phys. **406**, 152-172 (2019) doi:10.1016/j.aop.2019.04.007 [arXiv:1806.03719 [gr-qc]].
- [61] Y. C. Ong and Y. Yao, JHEP **10**, 129 (2019) [erratum: JHEP **12**, 164 (2019)] doi:10.1007/JHEP10(2019)129 [arXiv:1907.07490 [gr-qc]].
- [62] G. T. Horowitz, [arXiv:gr-qc/9301008 [gr-qc]].
- [63] C. Blaga, Serb. Astron. J. **190**, 41 (2015) doi:10.2298/SAJ1590041B [arXiv:1407.1504 [gr-qc]].
- [64] X. H. Feng, H. S. Liu, H. Lü and C. N. Pope, Phys. Rev. D **93**, no.4, 044030 (2016) doi:10.1103/PhysRevD.93.044030 [arXiv:1512.02659 [hep-th]].
- [65] C. Y. Wang, Y. F. Shen and Y. Xie, JCAP **04**, 022 (2019) doi:10.1088/1475-7516/2019/04/022 [arXiv:1902.03789 [gr-qc]].